CORRELATING LOCAL LONG AND SHORT RANGE SCATTERERS IN GRAPHENE PROPERTIES

Author:

Sajjad Tollabimazraehno

Supervisors:

Prof. Micheal F. Crommie, UCB
Prof. Kurt Hingerl, JKU

Report

in the visiting

Abstract

The garaphne flake has been prepared by mechanical exfoliation from high quality HOPG and transferred on BN/SiO_2 substrate in procedure called "Dry Transfer". The Au/Cr electrodes were written and deposited by electron lithography and e-beam evaporation, respectively. Transport measurements have been done right after lift-off, annealing in H_2/Ar at $350°C$ for 3.5 hours, after transferring the sample inside the UHV-STM chamber and after each current annealing interval.

Conductivity versus back gate voltage has a higher slope after each step, which indicates better mobility in graphene. Dirac point moved towards zero gate voltage after annealing graphene in H_2/Ar and higher value for minimum conductivity at Dirac point. The effect of current annealing to removing dielectric ice layer as a short-range scatterer and charged impurity as a long-range scatterer, and transport on graphene has been studied.

Acknowledgements

Contents

List of Figures

Chapter 1

Graphene electronic properties

1.1   Introduction

One of the most important physical properties of carbon based systems is the dimensionality of structures, because of the flexibility of its bonding. Graphene which is look like composed of free hydrogen benzene rings, a tow dimensional allotrope of carbon atoms in honeycomb structure, is important because it is the basis to understand the electronic properties of other allotropes. Graphite, which is well known as a pencil and useful for writing, is the stacks of graphene layers that are weakly coupled by van der Waals forces. Although graphene can be a product of writing on a paper by pencil and no one expected to graphene to exist in the free state until Novoselov and et al [9] find it on SiO_2 by optical microscope [10–12]. Rolling graphene along the specific direction and connecting the carbon bonds can cause well known one dimensional carbon nanotubes [13, 14]. Finally, zero dimensional spherical carbon system, Fullerenes [15]with discrete energy states can be obtained by wrapped-up graphene.

Carbon atoms in Graphene have σ bond with other carbon atoms and sp^2 hybridization, separated 1.42 Å from each other. The unaffected p orbital, which is perpendicular to the graphene lattice, can form the π band with other carbon atoms figure 1.1. P. R. Wallace was the first author who wrote on graphene band structure in 1946 and showed the anomalous semimetallic behavior in graphene [16]. Some of most interesting aspects of graphene are its low energy excitation are massless, Dirac fermions, chiral, chemical potential crosses the Dirac point and the anomalous integer quantum Hall effect at room temperature [17–19].

By understanding and control graphene's unusual structural and electronic flexibility can open doors for a new frontier in electronics.
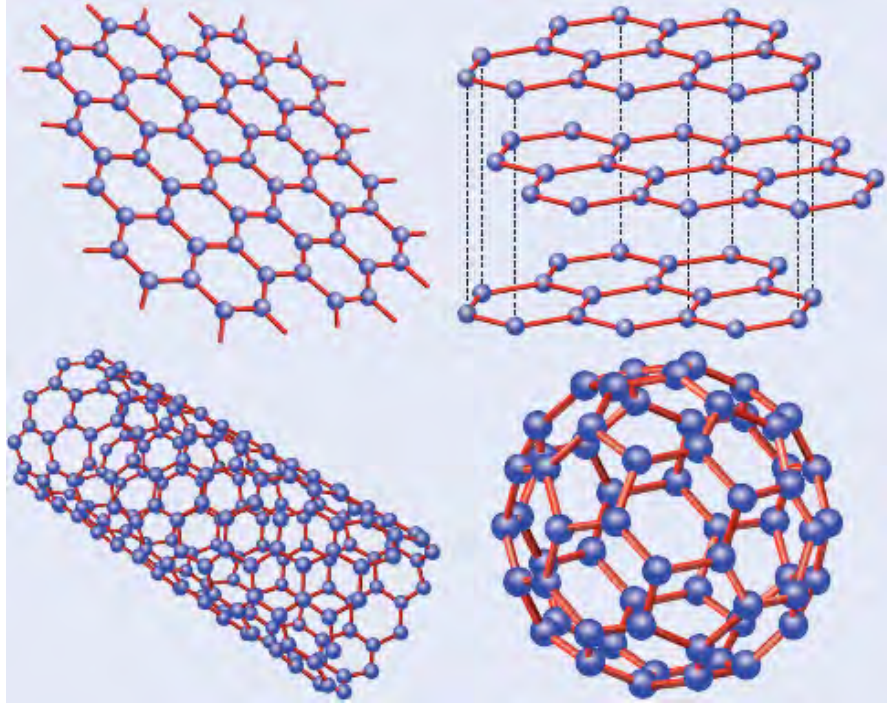
FIGURE 1.1: (Top left)Graphene honeycomb lattice (top right) Graphen stack or Graphite (bottom left) rolled-up graphene or Carbon nanotube (bottom right) wrapped graphene or Fullerenes (C60) [1]

1.2 Graphene lattice

Graphene is the mono-layer of carbon atoms in hexagonal structure arrangement figure 1.2 which is the triangular lattice with tow atoms in basis. Carbon atom bonds are 1.42 Ålong and 120° apart. The lattice vectors can be written as

$$a_1 = \left(\frac{3a}{2}, \frac{a\sqrt{3}}{2} \right), \qquad a_2 = \left(\frac{3a}{2}, -\frac{a\sqrt{3}}{2} \right) \tag{1.1}$$

Where the length of the vectors are 2.46 Å. While the relation between real and reciprocal space is

$$b_1 = 2\pi \frac{a_2 \times z}{|a_1 \times a_2|}, \qquad b_2 = 2\pi \frac{z \times a_1}{|a_1 \times a_2|} \tag{1.2}$$

$$\tag{1.3}$$

Therefor, the reciprocal lattice vectors are given by

$$b_1 = \frac{2\pi}{3a} \left(1, \sqrt{3} \right), \qquad b_2 = \frac{2\pi}{3a} \left(1, -\sqrt{3} \right) \tag{1.4}$$

The reciprocal lattice vectors can construct the hexagonal Bravias lattice in k space figure 1.2. There are three nearest and six second nearest neighbors in honeycomb geraphene lattice.
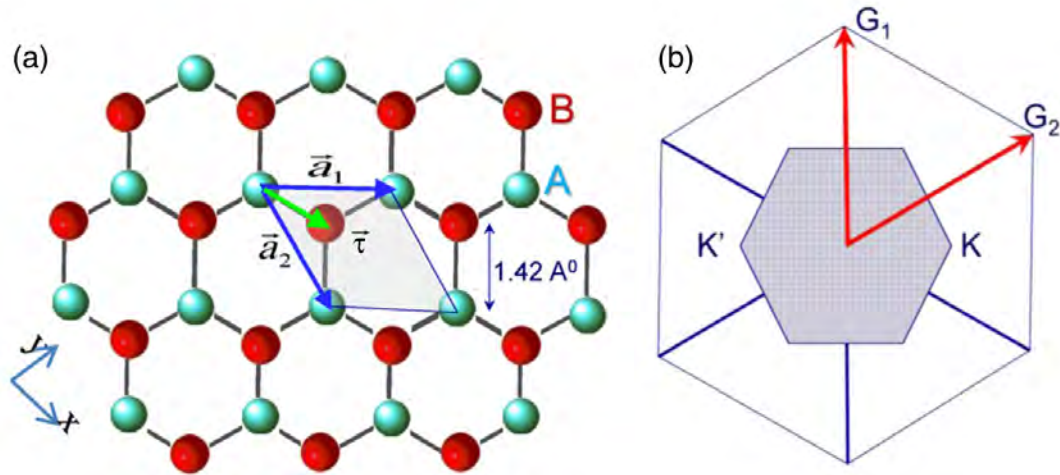
FIGURE 1.2: Graphene lattice. (a)Honeycomb structure with lattice unit vector a_1 and a_2 and tow atoms in sublattice A and B. (b) Brillouin zone in reciprocal space [2]

1.3 Tight-binding model

Physicist use tight binding model to calculate the electronic band structure in solid state physics. The approximate set of wave functions based on superposition of individual atom Bloch functions at each atomic site are used to calculate the band structure. The wave functions, which are similar to the atomic orbitals, belong to electrons that are tightly bound to its own atoms and do not interact with each other. In this model interaction of electrons with one another and potentials are neglected, therefore the ionization energy is rather close to the electron energy in isolated atom figure 1.3.

To obtain the the true Hamiltonian "H" of system, the corrections in lattice potential are assumed small therefor:

$$H(r) = \sum_i H_{at}(r - r_i) + V(r) \tag{1.5}$$

An approximation of linear superposition of atomic orbitals $\varphi(r - r_i)$ which are the eigenfunctions of a single isolated atom Hamiltonian, employs as a solution of time independent single electron Schrodinger equation:
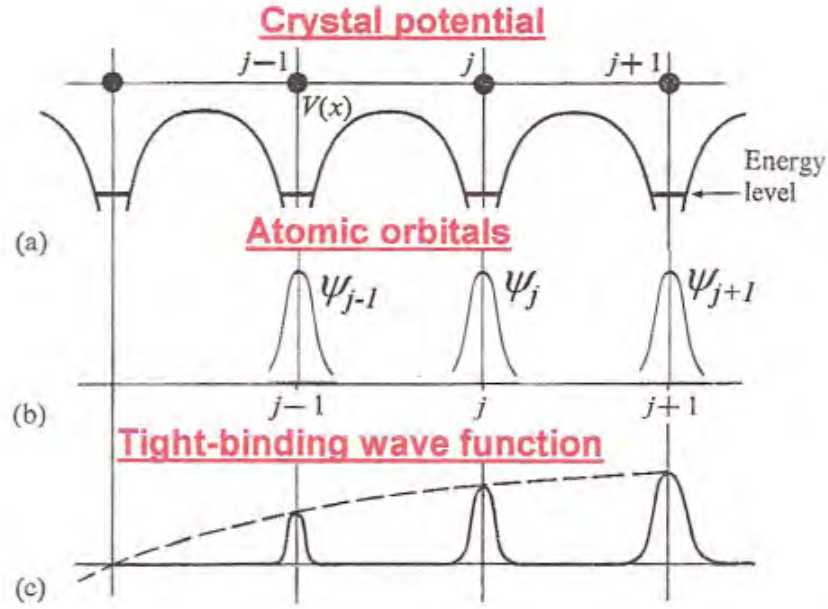
FIGURE 1.3: (a)The crystal potential. (b)Atomic wave function. (c) Corresponding Bloch function in tight binding model. [3]

$$\psi(r) = \sum_{i,j} c_j(r_i)\varphi_j(r - r_i) \tag{1.6}$$

where i and j refer to an i_{th} atomic site and j_{th} atomic energy level. By considering the symmetry in Bloch theorem and normalizing the wave function to unity for the system with n atomic orbitals φ_j in unit cell:

$$\Phi_j(k,r) = \frac{1}{\sqrt{N}} \sum_{i}^{N} e^{ik.r_{ij}}\varphi_j(r - r_{ij}) \tag{1.7}$$

where r_{ij} denotes the position of the j_{th} orbital in the i_{th} unit cell and the sum is over N unit cells. In general, the electronic wave function $\Psi_j(k,r)$ is given by a linear superposition of the n different Bloch functions,

$$\Psi_j(k,r) = \sum_{l=1}^{n} c_{jl}(k)\Phi_l(k,r) \tag{1.8}$$

where c_{jl} are the expansion coefficient and the energy of the j_{th} band is given by,

$$E_j(k) = \frac{< \Psi_j|H|\Psi_j >}{< \Psi|\Psi >} \tag{1.9}$$

where H is the Hamiltonian and by substituting the wave function equation (1.8) into the energy gives,

$$
\begin{aligned}
E_j(k) &= \frac{\sum\limits_{i,l}^{n} c_{ji}^* c_{jl} < \Phi_i|H|\Phi_l >}{\sum\limits_{i,l}^{n} c_{ji}^* c_{jl} < \Phi_i|\Phi_l >} \tag{1.10} \\
&= \frac{\sum\limits_{i,l}^{n} H_{il} c_{ji}^* c_{jl}}{\sum\limits_{i,l}^{n} S_{il} c_{ji}^* c_{jl}} \tag{1.11}
\end{aligned}
$$

where transfer integral matrix elements H_{il} and overlap integral matrix elements S_{il} are defined by,

$$H_{il} =< \Phi_i|H|\Phi_l >, \qquad S_{il} =< \Phi_i|\Phi_l > \tag{1.12}$$

by minimizing the energy E_j with respect to c_{jm}^* gives,

$$\frac{\partial E_j}{\partial c_{jm}^*} = \frac{\sum_l^n H_{ml} c_{jl}}{\sum_{i,l}^n S_{il} c_{ji}^* c_{jl}} - \frac{\sum_{i,l}^n H_{ml} c_{ji}^* c_{jl} \sum_l^n S_{il} c_{jl}}{\left(\sum_{i,l}^n S_{il} c_{ji}^* c_{jl}\right)^2} = 0 \tag{1.13}$$

Substituting the energy equation (1.11),

$$\sum_{l=1}^{n} H_{ml} c_{jl} = E_j \sum_{l=1}^{n} S_{ml} c_{jl} \tag{1.14}$$

H is defining as the transfer integral matrix, S as the overlap integral matrix and Ψ_j as a column vector,

$$H = \begin{pmatrix} H_{1,1} & H_{1,2} & \cdots & H_{1,n} \\ H_{2,1} & H_{2,1} & \cdots & H_{2,n} \\ \vdots & \vdots & \ddots & \vdots \\ H_{n,1} & H_{n,2} & \cdots & H_{n,n} \end{pmatrix}$$

$$S = \begin{pmatrix} S_{1,1} & S_{1,2} & \cdots & S_{1,n} \\ S_{2,1} & S_{2,1} & \cdots & S_{2,n} \\ \vdots & \vdots & \ddots & \vdots \\ S_{n,1} & S_{n,2} & \cdots & S_{n,n} \end{pmatrix}$$

$$\Psi_j = \begin{pmatrix} c_{j1} \\ c_{j2} \\ \vdots \\ S_{jn} \end{pmatrix}$$

equation (1.14) to be expressed as

$$H\Psi_j = E_j S\Psi_j \tag{1.15}$$

To determine the energy one should solve the equation

$$det(H - E_j S) = 0 \tag{1.16}$$

1.3.1 Energy spectrum of single layer graphene in tight binding model

Carbon atoms have six electrons that four of them are in valance band. Three of them contribute to σ bound, the orbitals are sp^2 hybridized and the last one is in p_z orbital which is perpendicular to the graphene plane, and taking into account one $2p_z$ orbital per atomic site. There are tow atom sites in graphene unit cell, therefor model includes tow Bloch functions. Substituting the Bloch function equation (1.7) into the transfer integral definition equation (1.12), we can write the diagonal matrix element correspond to first sublattice as

$$H_f = \frac{1}{N}\sum_{i=1}^{N}\sum_{j=1}^{N} e^{ik.(r_{f,j}-r_{f,i})} < \phi_f(r - r_{f,i})|H|\phi_f(r - r_{f,j}) > \tag{1.17}$$

If we consider the dominant contribution arises from $i = j$ within every unit cell, the matrix element $< \phi_f|H|\phi_f >$ has the same value on every first site which is equal to the $2p_z$ orbital

$$\epsilon_{2p} =< \phi_f(r - r_{f,i})|H|\phi_f(r - r_{f,j}) > \tag{1.18}$$

$$H_{ff} \approx \frac{1}{N} \sum_{i=1}^{N} \epsilon_{2p} \approx \epsilon_{2p} \tag{1.19}$$

There is no difference between carbon atoms in the lattice and they are chemically identical. Therefor, for the second sublattice atomic site has the same structure as the first one, it means for the diagonal transfer integral matrix element we have $H_{ff} = Hss \approx \epsilon_{2p}$ and

$$< \phi_f(r - r_{f,i})|\phi_f(r - r_{f,j}) >= 1 \tag{1.20}$$

$$
\begin{aligned}
S_{ff} = S_{ss} \;\; &= \;\; \frac{1}{N} \sum_{i=1}^{N} \sum_{j=1}^{N} e^{ik.(r_{f,j}-r_{f,i})} < \phi_f(r - r_{f,i})|\phi_f(r - r_{f,j}) > \tag{1.21} \\
&\approx \;\; \frac{1}{N} \sum_{i=1}^{N} e^{ik.(r_{f,j}-r_{f,i})} < \phi_f(r - r_{f,i})|\phi_f(r - r_{f,j}) > \tag{1.22} \\
&= \;\; \frac{1}{N} \sum_{i=1}^{N} \tag{1.23} \\
&= \;\; 1 \tag{1.24}
\end{aligned}
$$

In order to calculate the off-diagonal matrix element, we substitute the Bloch function equation (1.7) into the transfer integral equation (1.12) which is the hopping between first (f) and second (s) sublattices. This hopping term arises from interaction between nearest neighbors and we have the summation over all of the sublattice basis. Every atom in graphene lattice has three nearest neighbors, so, the second summation will be $l = 1...3$. The hopping term for each neighboring pair has the same value and it is independent of indexes. Then, it is set to "t" parameter which is negative [14], so, $\gamma_0 = -t = - < \phi_f(r - r_{f,i})|H|\phi_s(r - r_{s,l}) >$. That gives,

$$H_{fs} \approx \frac{1}{N} \sum_{i=1}^{N} \sum_{l=1}^{3} e^{ik.(r_{s,l}-r_{f,i})} < \phi_f(r - r_{f,i})|H|\phi_s(r - r_{s,l}) > \tag{1.25}$$

$$\approx -\frac{1}{N} \sum_{i=1}^{N} \sum_{l=1}^{3} e^{ik.(r_{s,l}-r_{f,i})} \gamma_0 \tag{1.26}$$

$$= -\frac{\gamma_0}{N} \sum_{i=1}^{N} \sum_{l=1}^{3} e^{ik.\delta_l} \equiv -\gamma_0 f(k) \tag{1.27}$$

$$f(k) = \sum_{l=1}^{3} e^{ik.\delta_l} \tag{1.28}$$

$$\delta_l = r_{sl} - r_{fi} \tag{1.29}$$

For three nearest neighbors, there are three vectors

$$\delta_1 = \left(0, \frac{a}{\sqrt{3}}\right), \quad \delta_2 = \left(\frac{a}{2}, -\frac{a}{2\sqrt{3}}\right), \quad \delta_3 = \left(-\frac{a}{2}, -\frac{a}{2\sqrt{3}}\right) \tag{1.30}$$

$$|\delta_1| = |\delta_|| = |\delta_3| = \frac{a}{\sqrt{3}} \tag{1.31}$$

$$f(k) = \sum_{l=1}^{3} e^{ik.\delta_l} \tag{1.32}$$

$$= e^{\frac{ik_y a}{\sqrt{3}}} + e^{\frac{ik_x a}{\sqrt{2}}} e^{-\frac{ik_y a}{2\sqrt{3}}} + e^{-\frac{ik_x a}{2}} e^{-\frac{ik_y a}{2\sqrt{3}}} \tag{1.33}$$

$$= e^{\frac{ik_y a}{\sqrt{3}}} + 2e^{-\frac{ik_y a}{2\sqrt{3}}} cos(\frac{k_x a}{2}) \tag{1.34}$$

The other off-diagonal matrix element H_{sf} is the complex conjugate of H_{fs}:

$$H_{fs} \approx -\gamma f(k), \quad H_{sf} \approx -\gamma f^*(k) \tag{1.35}$$

The off-diagonal overlap integral matrix element is given,

$$S_{fs} = \frac{1}{N}\sum_{i=1}^{N}\sum_{j=1}^{N} e^{ik.(r_{s,j}-r_{f,i})}\langle\phi_f(r-r_{f,i})|\phi_f(r-r_{s,j})\rangle \tag{1.36}$$

$$\approx \frac{1}{N}\sum_{i=1}^{N}\sum_{l=1}^{3} e^{ik.(r_{s,l}-r_{f,i})}\langle\phi_f(r-r_{f,i})|\phi_f(r-r_{s,j})\rangle \tag{1.37}$$

$$= s_0 f(k) \tag{1.38}$$

where $s_0 = \langle\phi_f(r-r_{fi})|\phi_s(r-r_{sl})\rangle$ and $S_{sf} = S_{fs}^* = s_0 f^*(k)$.Therefor, the transfer integral matrix elements and overlap integral matrix elements give

$$H = \begin{pmatrix} \epsilon_{2p} & -\gamma_0 f(k) \\ -\gamma_0 f^*(k) & \epsilon_{2p} \end{pmatrix}$$

$$S = \begin{pmatrix} 1 & s_0 f(k) \\ s_0 f^*(k) & 1 \end{pmatrix}$$

where $\gamma = 3.033eV$, $s_0 = 0.129$ and $\epsilon_{2p} = 0$ [14]. Energy E might be determined by solving $det(H_1 - ES_1) = 0$ so,

$$det\begin{pmatrix} \epsilon_{2p} - E & -(\gamma_0 + Es_0)f(k) \\ -(\gamma_0 + Es_0)f^*(k) & \epsilon_{2p} - E \end{pmatrix} = 0$$

$$E_{\pm} = \frac{\epsilon_{2p} \pm \gamma_0|f(k)|}{1 \mp s_0|f(k)|} \tag{1.39}$$

and by considering hopping the electron to second nearest neighbor atoms with the hopping energy t' $(0.02t \lesssim t' \lesssim 0.2t)$ [20] $t' \approx 0.1eV$ [21] that the t is nearest neighbor hopping energy $t \approx 2.8eV$ [16]

$$E_{\pm}(k) = \pm\sqrt{3 + h(k)} - t'h(k) \tag{1.40}$$

$$E(k) = 2cos\left(\sqrt{3}k_y a\right) + 4cos\left(\frac{\sqrt{3}}{2}k_y a\right)cos\left(\frac{3}{2}k_x a\right) \tag{1.41}$$

The calculated band structure is shown in figure 1.4 in the vicinity of Brillouin zone. A cut through the band structure shown in figure 1.5 where the band is plotted as a function of k_x where the Fermi level is located at zero energy for pure graphene.
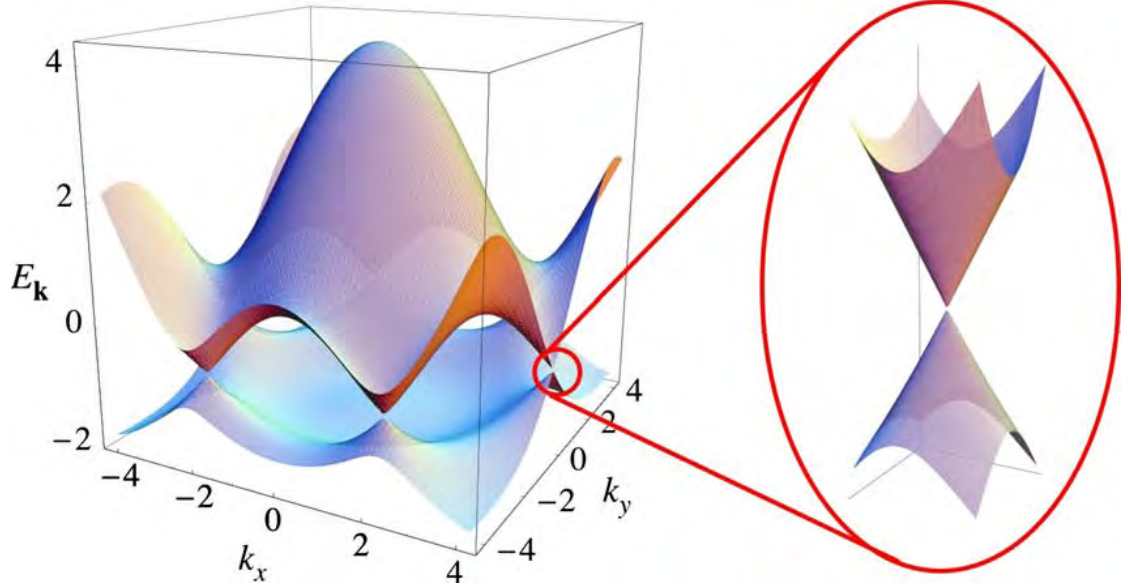
FIGURE 1.4: (left)Tight binding calculation for energy spectrum in graphene honeycomb lattice (right) low energy electronic bands of monolayer graphene at Dirac points for $t' = 0$ [4]

There is no band gap between valence band (E_-) and conduction band (E_+) and they cross at six corners of Berillouin zone figure 1.4 (left) that are known as K points. Near this points the electronic dispersion is linear figure 1.4 (right) and can be described by Dirac like Hamiltonian.

1.3.2 Density of state in single layer graphene

The Hamiltonian for electrons in graphene that electrons can hop to nearest and second nearest neighbor atoms in tight binding model has the form

$$H = -t \sum_{\langle i,j \rangle, \sigma} \left(a_{\sigma,i}^\dagger b_{\sigma,j} + H.c. \right) - t' \sum_{\langle i,j \rangle, \sigma} \left(a_{\sigma,i}^\dagger a_{\sigma,j} + b_{\sigma,i}^\dagger b_{\sigma,j} + H.c. \right) \tag{1.42}$$

where $a_{\sigma,i}^\dagger$ and $a_{\sigma,i}$ creates and annihilates an electron[16]. The density of state per unit cell can be obtain by deriving from equation (1.42) which is given for $t' = 0$ and $t' \neq 0$ in figure 1.6 that behave in both cases like semimetallic [16, 22]. For $t' = 0$ [23]
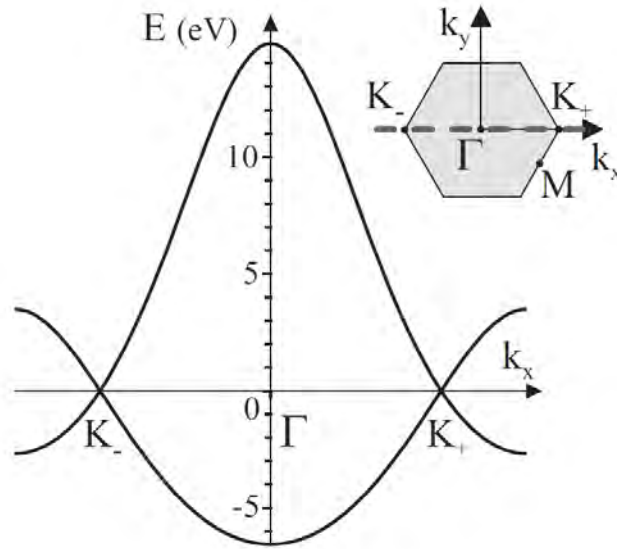
FIGURE 1.5: (left)Tight binding calculation for energy spectrum in graphene honey-comb lattice (right) low energy electronic bands of monolayer graphene at Dirac points for $t' = 0$ [5]
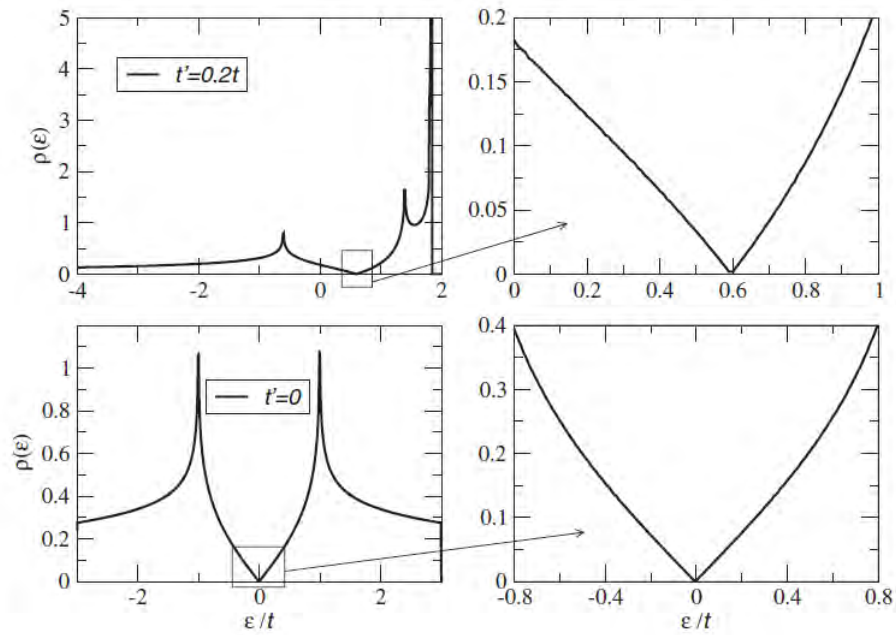
FIGURE 1.6: Computed density of states as a function of energy per unit cell from the dispersion energy, and zoom in of density of states close to the Dirac point (neutrality point), close to the neutrality point $\rho(\epsilon) \propto |\epsilon|$ for $t' = 0$ [4]

$$\rho(E) = \frac{4|E|}{\pi^2 t^2 \sqrt{Z_0}} \mathbf{F}\left(\frac{\pi}{2}, \sqrt{\frac{Z_1}{Z_0}}\right) \tag{1.43}$$

where $\mathbf{F}(\pi/2, x)$ is the complete elliptic of the first kind. The density of state per unit cell close to the Dirac point is given by

$$\rho(E) = \frac{2A_c|E|}{\pi v_F^2} \tag{1.44}$$

where v_F is the Fermi velocity, with value $v_F \approx 1 \times 10^6 m/s$ [16] and $A_c = 3\sqrt{3}a^2/2$ is the unit cell area.

1.4 The integer quantum hall effect in single layer graphene

Electrons in tow dimensional electron system follow circular cyclotron orbits in applied magnetic field. The Hall conductivity and their allowed energies will be quantized into values known as Landau levels [24]. The Landau levels spectrum for single layer graphene was calculated about sixty years ago by McClure [25] and the integer quantum Hall effect observed [17, 18] recent years.

Tow dimensional electron gas system in low magnetic field, the circular orbits will quantized and the Landau levels give rise to quantum oscillation known as Shubnikov–de Haas oscillations and the de Haas–van Alphen effect. The energy of these levels will discrete to $E_n = \hbar\omega(n + 1/2)$, where $\omega = eB/m$ is cyclotron frequency figure 1.7 and the lowest energy state will be $E = \hbar\omega/2$.

In higher magnetic field, by considering the spin effect on energy degeneracy, it will add twofold degeneracy. Then plenteous will occur on quantized conductance values

$$\sigma_{xy} = \frac{I_{channel}}{V_{Hall}} = N\left(g\frac{e^2}{h}\right) \tag{1.45}$$

where N is an integer number and e^2/h is the quantum of conductance, therefor there is distance equal to ge^2/h between the plateaus and the distance between the σ_{xy} on density axes is gB/ϕ_0 which is the maximum carrier density per Landau levels and $\phi_0 = h/e$ is the quantum of flux.

Graphene single layer has degenerate fourfold Landau levels that rises from spin (twofold) and valley (twofold). The quantized plateaus are separated by $4e/h$ in integer quantum Hall conductivity, but plateaus will occur at half integer value of $4e/h$ figure 1.8
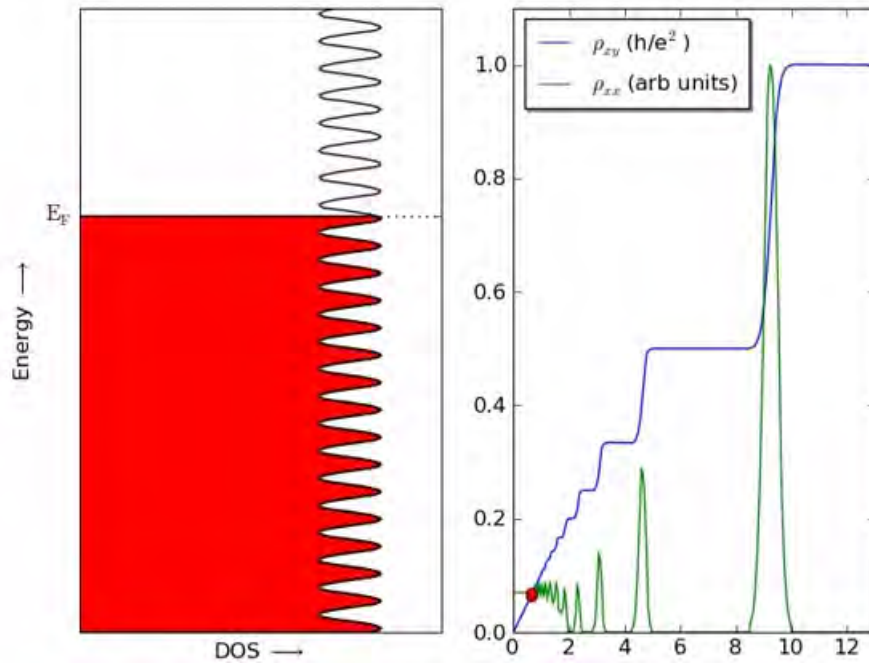
FIGURE 1.7: Quantum oscillation of Landau levels in low magnetic field for 2-D electron system

$$\sigma_{xy} = -\frac{1}{2}\left(2N + 1\right)\left(4\frac{e^2}{h}\right) \tag{1.46}$$

For the semi classical approximation produces the energy sequence:

$$E_N = \pm\sqrt{2e\hbar v_F^2 B|N|} \tag{1.47}$$

where $N = 0, \pm 1, \ldots$ and $\pm$ refers to electron and hole sectors, respectively figure 1.9.
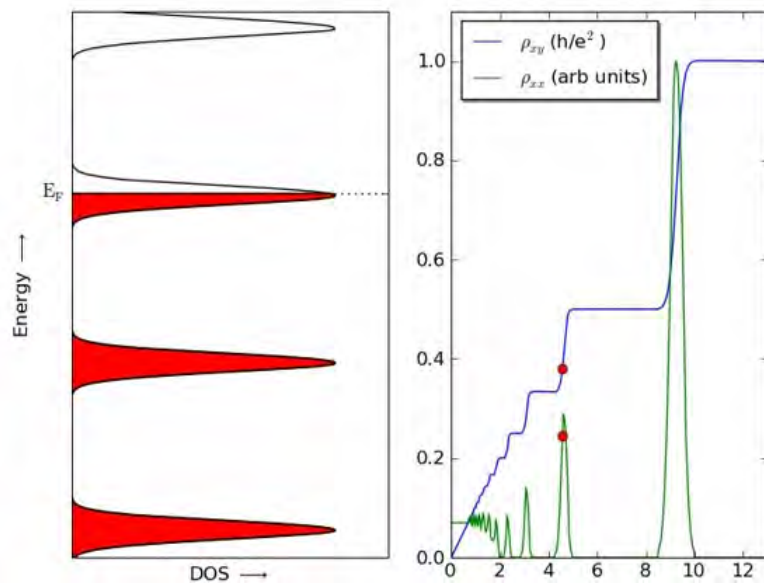
FIGURE 1.8: Integer quantum Hall effect in high magnetic field, plateaus separated by $4e/h$
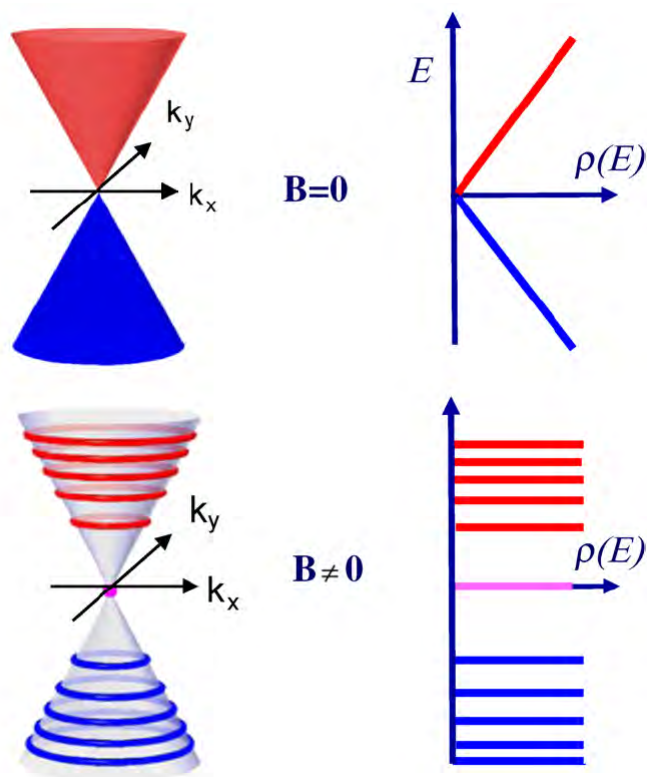
FIGURE 1.9: (Top) DOS and low energy dispersion in zero magnetic field for electrons (red) and holes (blue) (Bottom) DOS and energy dispersion in high magnetic field exhibits a discrete levels and DOS consists of a sequence $\delta(E - E_n)$ [2]

Chapter 2

Fabrication

2.1 *Graphene/BN/Sio$_2$*

Fabrication is a vital component in transport and STM measurements. The sample was a single layer of graphene on Boron Nitride (BN) on SiO_2. First of all, the BN layer which has almost the same graphene lattice, were transferred by exfoliation process on SiO2. Silicon oxide wafer has a thermal oxide of Si in both side with the thickness of $270nm$. After transferring the BN the graphene flakes were transfer in process called "Dry Transfer". Finally, couple of Au/Cr electrodes were evaporated on graphene after writing them by electron lithography in order to do the transport measurement inside the UHV-STM.

2.1.1 *BN/SiO$_2$* by mechanical exfoliation

We use the hexagonal crystal of boron nitride among the BN polymorphous. This $h-BN$ crystal has the hexagonal lattice parameter close to graphene and strong ionic bond in lattice plane. $h-BN$ is relatively inert and the planar surface suppress rippling and wrinkles in graphene [26, 27] and free of dangling bonds and surface charge traps [28] therefor the graphene flake on h-BN is free of distortions and wrinkles figure 2.1.

In order to have a $h-BN$ flake with largest size on SiO_2 substrate. First, we cut the SiO_2 wafer in proper size about $1cm \times 1cm$ and wipe it with DI-water and IPA then dry it with nitrogen gas to have a clean surface. In second step, we put a few $h-BN$ crystals on adhesion side of a scotch tape and bring the clean area of tape to contact to BN flakes and pull it back. We repeat this process (7-10 times) to obtain a homogeneous distribution of thin BN flakes on Tape figure 2.2.
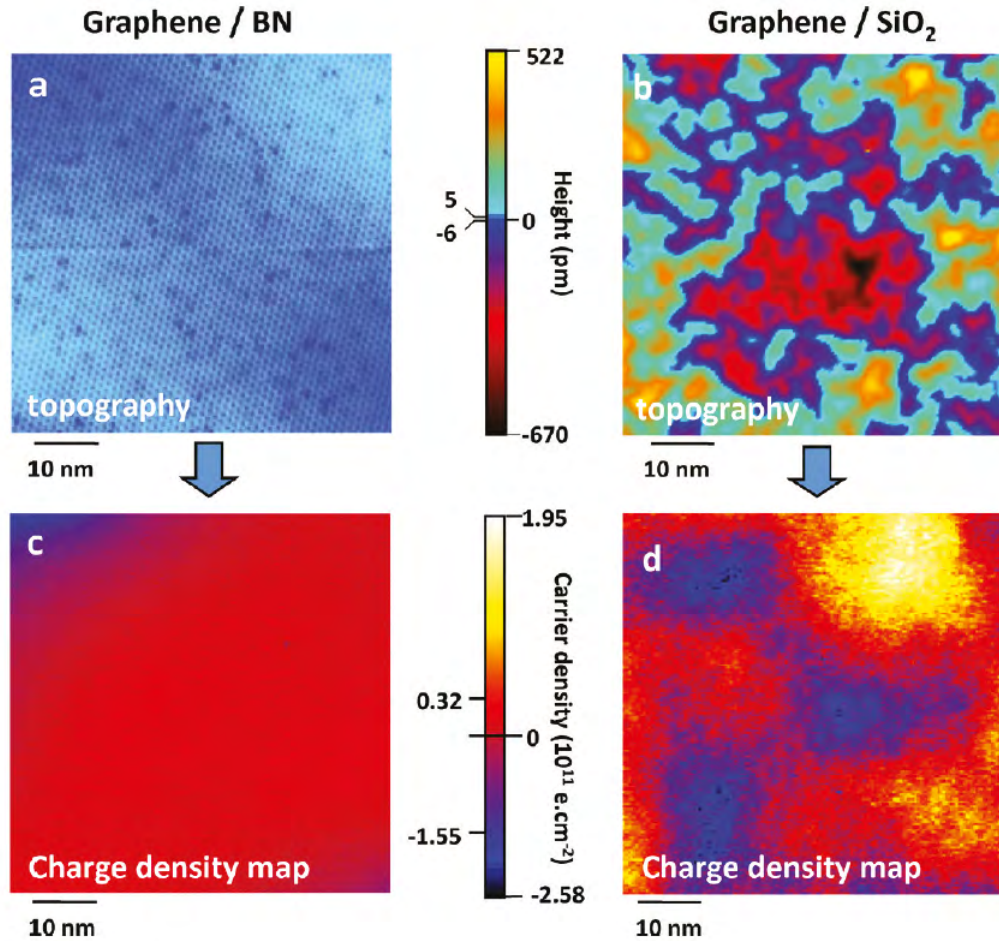
FIGURE 2.1: Topography and charge density for graphene on BN and SiO_2, STM image size $60nm \times 60nm$ [6]

We brought the area which is covered with lower amount of BN, into contact with clean SiO_2 surface. The tape area in contact with silicon oxide is gently brushed to avoid trapping air between tape and substrate and gently pressing the stack with the thumb a few times. In next step, we have to remove the tape very slow like $1cm/h$ otherwise you wont have any BN flakes on substrate figure 2.3.

Finally, we have to remove the residual adhesive part of the scotch tape. BN flakes on SiO_2 substrate will be annealed at $500°C$ for three hours in air. BN flake thickness can not be controlled in exfoliation while we need the flakes with thickness of $30nm$ which are blue in optical microscope on silicone oxide figure 2.4. The size of the flakes depend on primary size of the crystals and normally flakes are smaller than $30\mu m$, but we could produce the flakes larger than $120\mu m$.
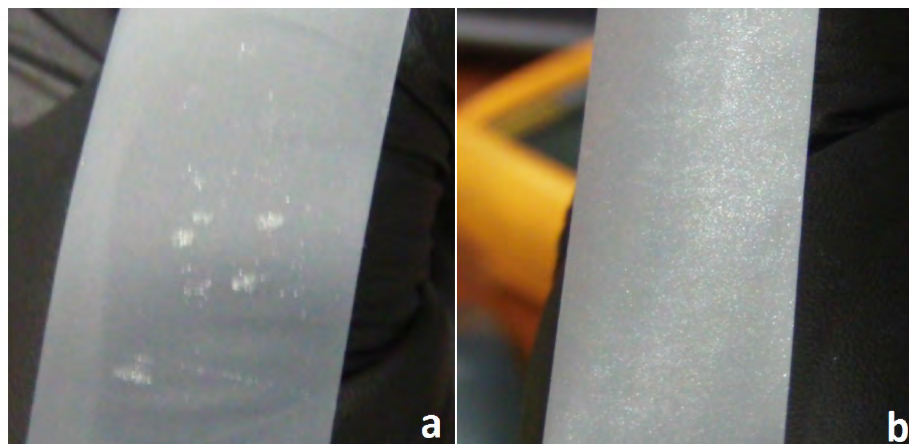
FIGURE 2.2: BN crystals (a) before and (b) after exfoliation
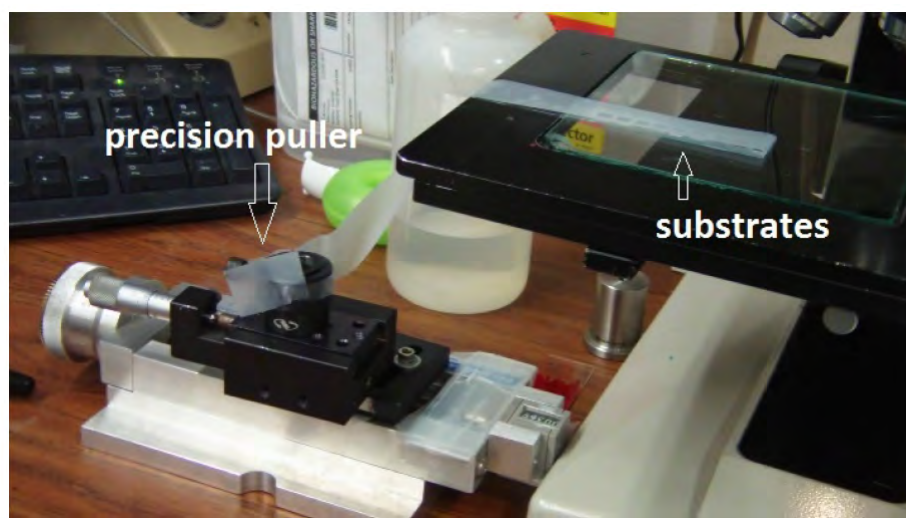
FIGURE 2.3: set up to remove the scotch tape slowly

2.2 Dry transfer of Graphene on BN

We attach the scotch tape on glass slide, without trapping air in between. Then, MMA is spin coated on tape/glass by putting one MMA droplet on surface and spin coat it at speed $3000rpm$ for 30 seconds. About $15cm$ of non transparent tape was removed and pressed firmly to the HOPG, from the adhesion side. The thick layer of graphite was gently peeled away by tape. Next step is similar to BN exfoliation, the clean part of adhesive section of the tape was folded upon the graphite section of tape. Tow layers were then pressed tightly together and then unfolded that the clean part of tape was covered by graphite. This processed was repeated until to get the gray area covered by graphite.

It was preferable that use the gray area, not the shiny section. The gray section was contacted to the MMA/tape/glass substrate and gently brush the whole area from one
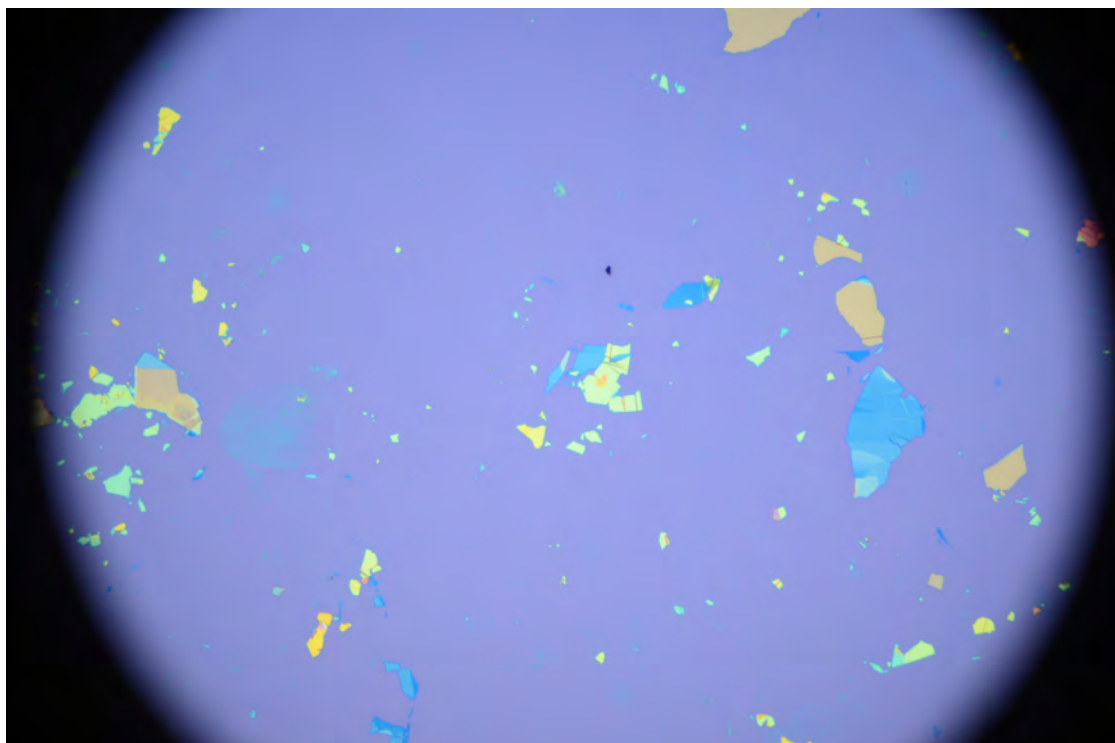
FIGURE 2.4: *BN* flakes on SiO_2 substrate, different colors represent the different thickness of BN

side towards the other side to get rid of all air in between. The tape was removed gently from one side (like BN transferring) really slowly. There are some graphene flakes on MMA that should transfer on BN. In order to find the single layer graphene flake which can be find from contrast, each sample was individually placed underneath the optical microscope by putting the black electrical tape on back side of glass slides. Single layer graphene has the less than 5% contrast difference with MMA figure 2.5.
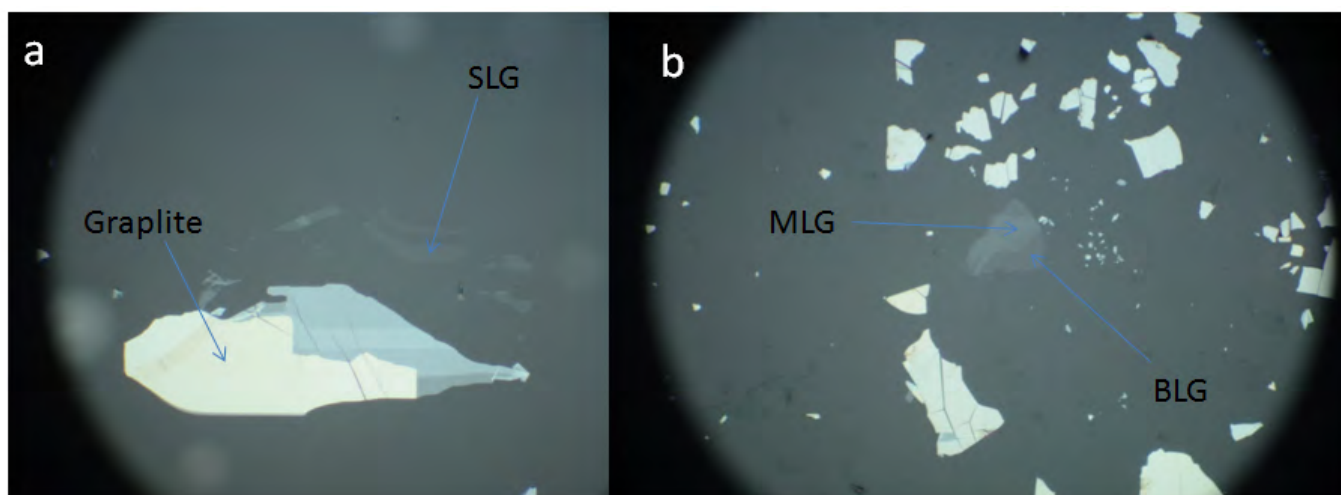
FIGURE 2.5: (a)Single layer graphene (SLG) has less that 5% contrast differences with MMA (b) Bilayer graphene (BLG) and Multilayer graphene (MLG)

Around the graphene flake was removed by cutting the tape on the glass to have a smaller area in order to find the SLG faster in next step. BN/SiO_2 was placed on transferring stage on heater then the blue BN flake was found at magnification 20X. SLG and BN were aliened by optical microscope and lowered the glass until the graphene flake was lay on the BN figure 2.6. The whole system were heated up to $120°C$ for 20 minutes. MMA/tape layer was removed by placing the silicon substrate with all layer in CH_2Cl_2 for 30 minutes.
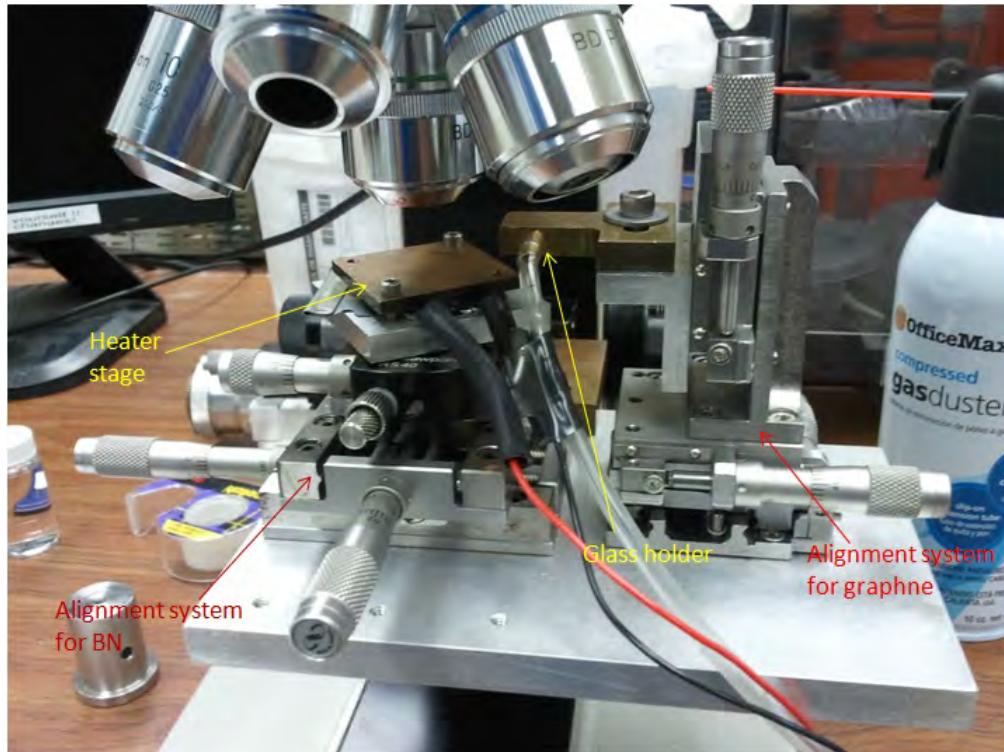
FIGURE 2.6: Micromanipulator alignment system for micrometer size graphene on BN with tens of micrometers size, BN/SiO_2 was placed on heater stage and the BN flake was found at the middle of microscope frame at 20X magnification, graphene/MMA was located beneath the glass holder and hold by vacuum, graphene was found and aligned on BN and lay on it by lowering the glass slide in Z direction

2.3 Fabrication of contacts

PMMA was deposited on substrate with graphene on top and exposed to electron bean to write the electrodes and connected wires. After writing the designed electrodes, sample was placed in MIBK to develop the electrodes and open the window for them. Au/Cr was evaporated by ebeam evaporation. PMMA was lifted off by acetone figure 2.7 and the residual PMMA on SLG was removed in next step. H_2 and Ar flow rate were set to $100sccm$ and $200sccm$ respectively, to build the pressure upto $1atm$ and stabilize the pressure by slowly opening the gate valve in the quartz tube. Temperature was set to

$350^{\circ}C$ and sample was annealed for 5 hours in this temperature. To see the parameters were used for lithography see [29].
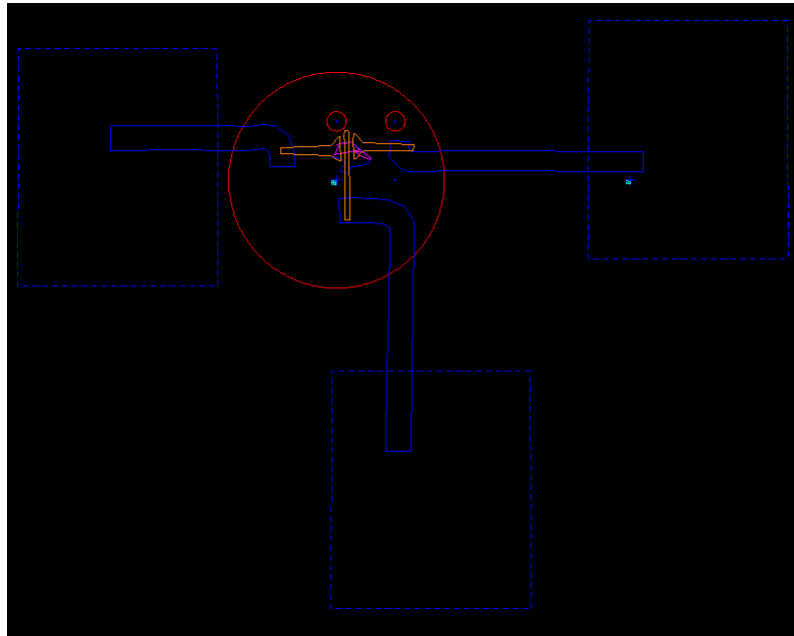
FIGURE 2.7: Electrodes and wires, the pink area is the graphene flake and micron size wires to make connection with external system for transport measurement

The gold electrodes were mounted on special sample plate for STM and wire bounded for transport measurement figure 2.8.

FIGURE 2.8: Sample plate; gold wires were wire bounded to sample plate electrodes; in order to have the back gate, the SiO_2 was scratched for wire bounding

Chapter 3

Tip Navigation in UHV-STM

3.1 Introduction

A sharp metallic tip scan the sample surface and record the surface topography as a function of tunneling current which depends exponentially on tip-sample distance,figure 3.1 by applying the voltage between tip and sample in scanning tunneling microscope (STM)[30]. Therefor, it is not possible to scan the non-conductive surfaces. Graphene flake is placed on insulator material with $10\mu m$ size on the substrate which is not conductive and graphene flake is too small.

One needs a coarse walker stage for tip navigation parallel and perpendicular to the sample surface that can follow the wires in by traveling in millimeter distances and change the tip-sample distance. The capacitance current proportionals to inverse of tip-sample distance and it is hard to find the electrode edges in higher distances, therefor in each step we have to approach the tip in tunneling regime and retract it. The smaller working distance does not favor due to the risk of tip crashing at high speed scanning although at higher working distance the resolution of edge detection is low, so, for narrower wire it is important to have the lower working distance. We used the long range optical microscope to find the biggest gold plate as a starting point for navigation.

3.2 Capacitance current measurement technique

There are terms in current flowing through the STM tip by applying ac modulation to the sample,
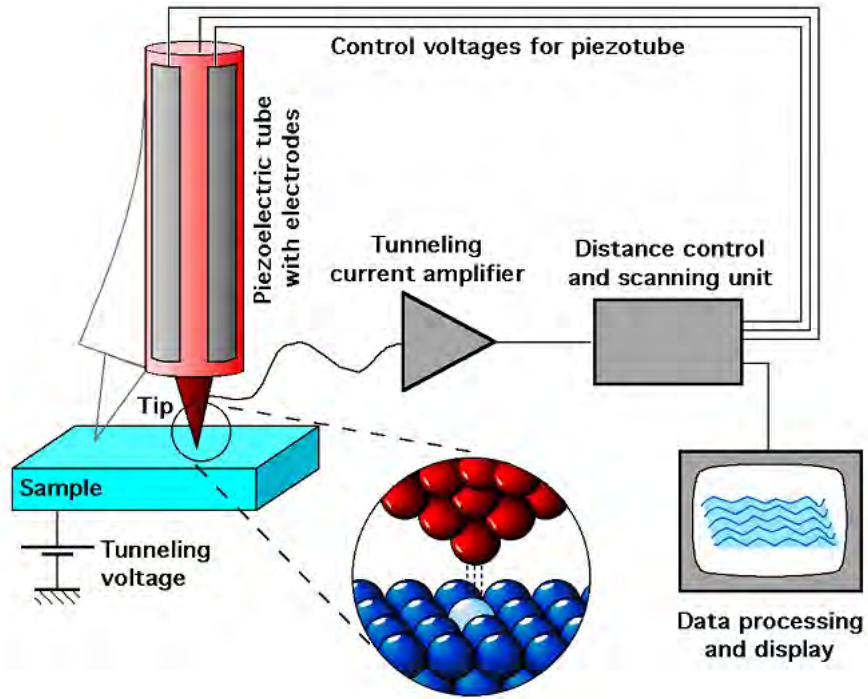
FIGURE 3.1: Schematic of Scanning Tunneling Microscope STM

$$I^{\sim} = G_t V_t^{\sim} + i\omega C V_s^{\sim} \qquad (3.1)$$

where G_t is the tunneling conductance and $V_s^{\sim}$ is the ac voltage. First term is from tunneling current and the second one from capacitance pickup current via tip-sample capacitance C. It is easy to distinguish capacitance pickup by retracting the tip from sample, not to be in tunneling regime. The tip-sample effective capacitance is in the range of $aF(10^{-18}F)$ when the tip is $3\mu m$ away from surface on the insulator and the background is in range of $fF(10^{-15}F)$ [7]. A good capacitance bridge setup needs to compensate the background to measure the small change in capacitance. It is worth to use the sample as a part of the bridge circuit figure 3.2 and one can tune the out-of-phase voltage $-V_{gate}^{\sim}$ to cancel the background current and variation of tip current is proportional to tip-sample capacitance.

The presence of back gate changes the electric field distribution around the sample, without back gate voltage the equipotential lines lose the shape of the sample quickly, and by grounding the back gate ($V_{gate} = 0$) the equipotential lines were pushed up. The equipotential lines change dramatically when the back gate voltage has the same magnitude but opposite sign, it develop strongly varying sharp feature above the edges which make it easy to distinguish at the comparable distance by the size of the wires
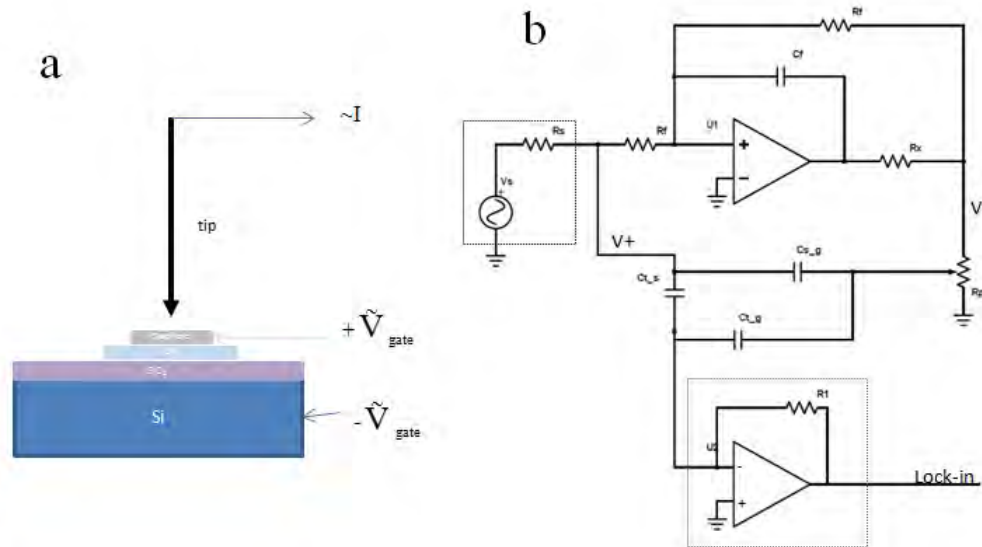
FIGURE 3.2: (a) Schematic experimental setup of back gate capacitance measurement (b) Equivalent circuit where $R_f = 5K\Omega$, $R_x = 10\Omega$, $R_p = 500\Omega$, $C_f = 5 - 20pF$ and Opamp $U_1 = AD843$. The output voltage from the lock-in amplifier splits into tow $180°$. One signal applied to the sample and the negative one to the back gate and measured capacitive pickup current through the same amplifier that is used for tunneling current

figure 3.3. The ac voltage applied to the sample and back gate was $200mV$ at $5kHz$ which is limited by the bandwidth of current amplifier $(10^9 V/A)$ using to measure tunneling current.
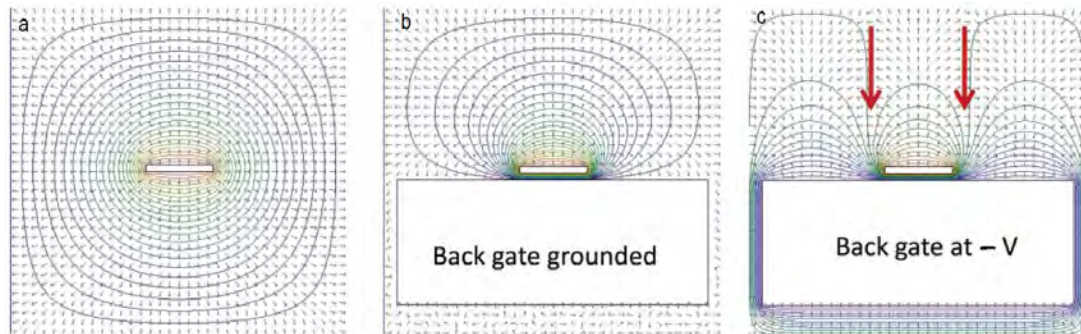
FIGURE 3.3: (a) Equivalent potential line near the conducting bar and the arrows show the field direction (b) The same bar nearby grounded back gate (c) The bare nearby back gate at negative voltage [7]

3.3 Micron size gold wire edge detection

As the tip moves across the gold wire, the variation capacitance current was plotted as a function of tip steps which correspond to the tip traveling distances. Although the pickup current and its spatial first derivatives dI/dx is shown in figure 3.4. The tow

turning points in first derivative correspond to the gold wire edges. The sharpness of the turning points decreases with increasing the tip-sample distance and it is getting more round and broader. However, to have the good resolution in edge detection, the tip-sample distance has to be comparable with wire's width. Therefor the distance/width ratio should be less than 0.3 to have a accurate edge identification. When the features become smaller, it is important to approach the tip to tunneling regime and retract it to obtain the desired resolution.
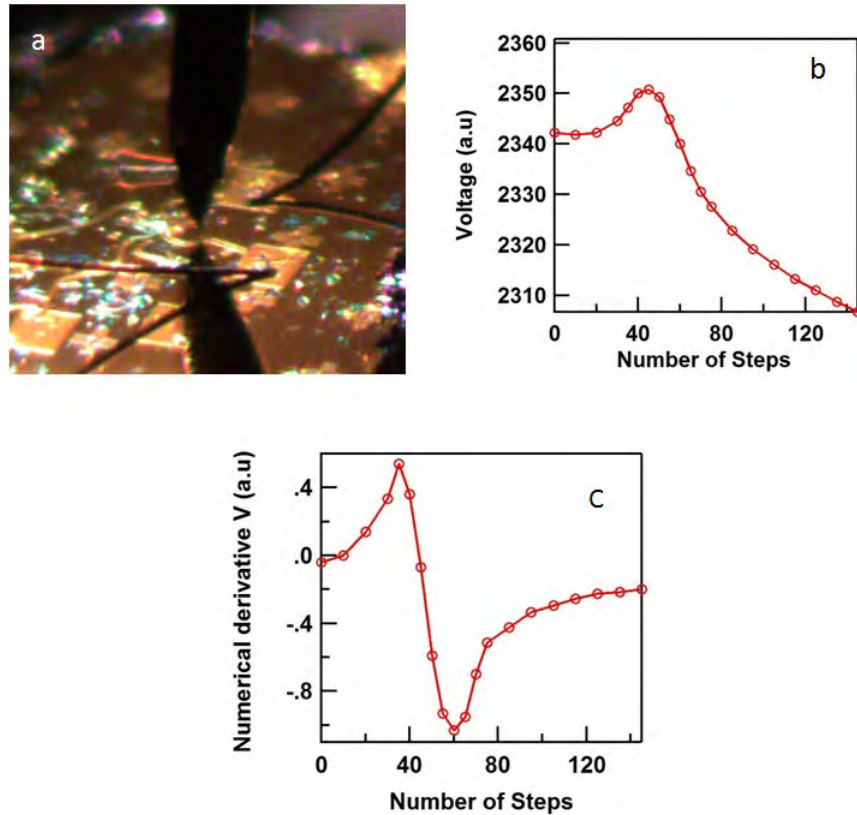
FIGURE 3.4: Variation of capacitance current as the tip moves across the gold wire (a) distance/width ratio less than 0.3, tip scanning the wire (b) Capacitance current converted to voltage in each tip step across the wire (c) First derivative of capacitance current dI/dx, tow turning points correspond to wire edges

3.4 Navigation protocol

First of all, we have to find the biggest gold plate and approach the tip next to the thinner wire which are connected to the plate, then retract the tip to a height correspond to aspect ration of 0.3 and phase lock it in lock-in. The main point is to identify the center of electrode from spatial derivative of capacitance current and move the tip along the gold wire to reach the graphene.

After phase lock, tip was moved towards the thinner wire and the capacitance current

was recorded as a function of tip steps when the program control the tip to move across the wire. The center of wire which is at the middle of tow turning point in first derivative was identified, scanning line must be tow times bigger that the wire width figure 3.5. We move the tip at center of wire and approach it. While the substrate is not horizontal perfectly, therefor, tip can crash during navigation because of the small slop. To avoid crashing, it is better to approach the tip and retract it again to be sure that the tip wont crash, after each edge detection. Sometimes the width of graphene flake is really small or the tow electrodes on graphene are too close that they interfere on capacitance measurements. In this case, it is better have the different width for electrode to make a good contrast finding graphene sample.
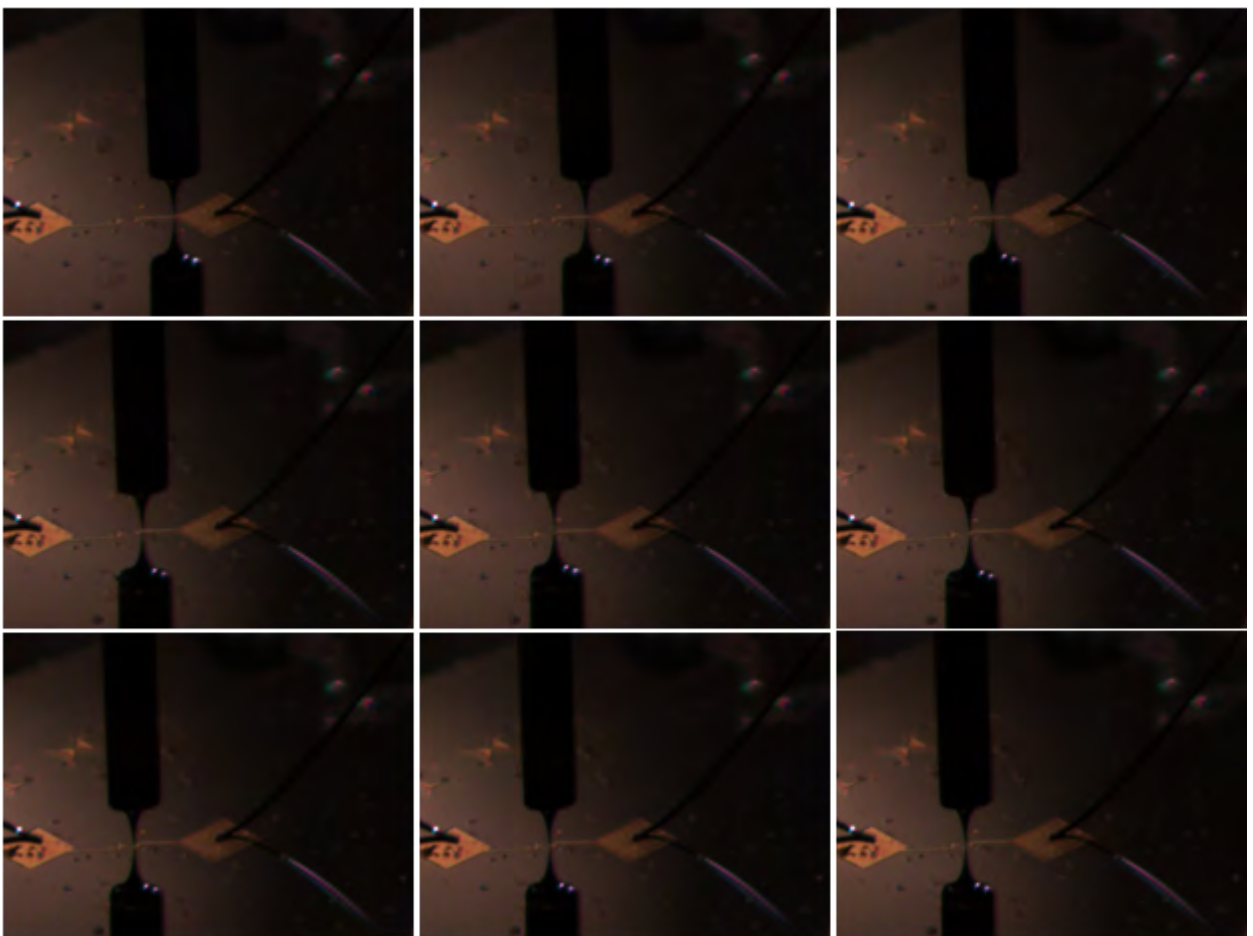
FIGURE 3.5: Tip navigation, images from top left to bottom right show the process tip navigation and in each step tip was approached and retracted to keep the safe distance, find the biggest gold electrode and approach on it then follow the smaller wire to finest one by scanning the width of wires and approaching to the middle of wire and retract it to reach the aspect ratio 0.3

Chapter 4

Transport in Graphene

4.1 Experiment

The STM measurements are performed in Ultra high vacuum condition $\sim 10^{-10} torr$ at room temperature. The aim of this measurement is to study and investigate the garpahene surface phenomenon during the transport measurement and the effect of parameters like current annealing on energy dispersion and graphene quality. Therefor, we measured the conductivity of graphene in each step. The transport measurements were performed after depositing gold electrodes, after annealing at $500°C$ for $3.5 hours$, after transferring the sample inside the UHV-STM chamber and after each current annealing step. It has been tried to remove the contaminants and ice by annealing the graphene at several hundreds Celsius [31, 32] in UHV. The graphene surface has been scanned after transferring the graphene in STM chamber and after each current annealing [33] to measure the surface roughness by STM. Graphene is able to carry high electric current without any damage $10^8 A/cm^2$ [33]. Such a high current through the graphene flake, which has micron size, can increase the temperate up to $600°C$, Joule heating, that can sublimate, desorb, melt or evaporate the remained impurities on the graphene surface.

4.2 Transport in Graphene

Novoselov, Tan and others [9, 17, 18, 34–36] explained unusual carrier density dependent conductivity $\sigma(n)$ in graphene and the minimum conductivity value (σ_{min}) which is twice the quantum unit of conductance $(4e^2/h)$, ripples in graphene [37] , short range disorder [38–41] and charge impurities [38, 39, 42–47].

The charge density of the sample can be tuned by applying a gate bias voltage Vg, and the electric field can dope the graphene by electrons or holes. The sample was measured using lock-in amplifiers at an excitation voltage less than $50\mu V$ to minimize any heating effect on the samples. figure 4.1 shows the non zero value of gate voltage (V_{Dirac}) at minimum conductivity that indicates the existence of unintentional doping of graphene [44] whose origin is the charge impurities. The charge carrier density in graphene induced by gate voltage can be obtain from $n = C_g (V_g - V_{Dirac})/e$ [34] in the presence of charge impurities where the gate capacitance $C_g = 115$ and $108aF/\mu m^2$ for SiO_2 and BN substrates, respectively.
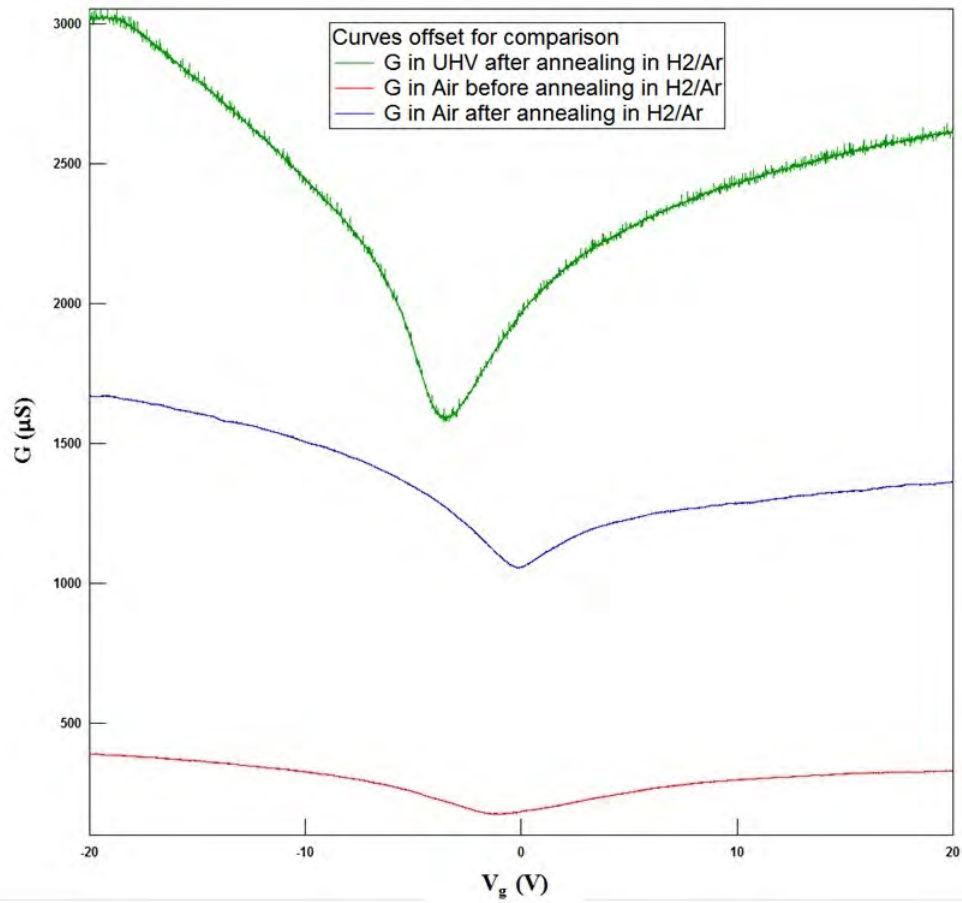
FIGURE 4.1: Conductance σ as a function of gate voltage V_g right after lift off, H_2/Ar annealing at $350°C$ and after transferring the sample in UHV-STM chamber before current annealing

The mobility increases after annealing the graphene at $350°C$ in air and figure 4.1 shows increasing in conductance and mobility after transferring the sample in UHV too. Dirac point moved towards the zero voltage after annealing while it is going far away from zero after transferring in UHV.

It is worth to have an estimation for mean free path of electrons an holes in graphene, by considering the scattering time $\tau = \hbar\sigma(\pi/n)^{1/2}/(e^2 v_f)$ and Fermi velocity $v_f \approx$

$10^6 m/s$ [48], resulting the mean free path range $10 - 500nm$ [34] for both holes an electrons which is strongly depends on charge density n. Numerical calculations showed that the conductance $\sigma(n)$ changes from linear to a sublinear dependence in graphene as the scattering mechanism changes from long-range scattering like charged impurity scattering to short-range scattering such as atomic defects in graphene lattice [39, 44].

4.3 Long-range scattering in Graphene

Nomura and et al and Hwang and et al [39, 44] showed that to scatter carriers, the long range impurity scattering is much more effective than short range to scatter carriers in 2D graphene system. For instance, the mean free path for short range scatterers is $\gtrsim 1\mu m$ while for the same impurity density $n_i \sim 5 \times 10^{11} cm^{-2}$, it is $\sim 50nm$ for charge impurities (long range scatterers) [34]. The Boltzmann transport theory with charged impurities can explain the conductivity since the size of the sample is several microns, so the diffusive regime can be considered for transport [38, 39, 42, 44–47],

$$\sigma(V_g) \approx \begin{cases} C\frac{e^2}{h}\frac{n}{n_i} & \text{for} n > n^* \\ C\frac{e^2}{h}\frac{n^*}{n_i} & \text{for} n < n^* \end{cases} \tag{4.1}$$

where C is a dimensionless numerical parameter describing the strength of scattering by impurities ($C \approx 20$ [42] for SiO_2 and $C \approx 36.4$ for BN substrate), n^* self consistent residual carrier density (electron and hole puddle formation induced by the charged impurities) and $n = C_g V_g/e + \bar{n}$ is the carrier density related to the gate voltage with $\bar{n}$ the induced carrier density in graphene by the charged impurity. n^* and $\bar{n}$ can be self-consistently determined by n_i and d, charge impurity concentration and distance between graphene flake and charge impurity [42]. Charged impurity scattering in graphene for $\sigma(V_g)$ when the V_g is not near $V_{g,min}$ can be expressed by,

$$\sigma(V_g) = \begin{cases} \mu_e C_g \left(V_g - V_{g,min}\right) + \sigma_{res} & \text{for} V_g > V_{g,min} \\ -\mu_h C_g \left(V_g - V_{g,min}\right) + \sigma_{res} & \text{for} V_g < V_{g,min} \end{cases} \tag{4.2}$$

where μ_e and μ_h are the electron and hole field-effect mobilities. Conductivity can be expressed as a function of carrier density

$$\sigma(n) = ge \mid \frac{n}{n_{imp}} \mid +\sigma_{res} \qquad (4.3)$$

where σ_{res} is the residual conductivity at n = 0 predicted in [46, 49] and $g = 5 \times 10^{15} V^{-1} s^{-1}$ is a constant.

equation (4.1) describes (1) the linear conductivity because of charge impurity scattering, (2) the minimum gate voltage $V_{g,min} = V_{Dirac} = -e\bar{n}/C_g$, owing to disorder due to charge impurities [39, 42, 44], (3) the minimum conductivity σ_{min} occurs at the carrier density which the average impurity potential is zero [42], not at the carrier density which neutralizes n_{imp}, and is given by $\approx 20e^2/h(n^*/n_i)$, (4) σ_{min} falls to the minimum value $4e^2/h$, by increasing n_{imp} that means the carrier density inhomogeneity is governed on σ_{min}, not the Dirac point singularity [36, 39, 44, 45] and (5) the plateau width.

Since equation (4.1) is only a function of impurity concentration, it might be possible to compare the clean graphene device, with low charge impurity density, and dirty sample. In clean sample, conductivity versus gate voltage has a higher slope, smaller V_{Dirac} (closer to zero), narrower minimum conductivity plateaus and higher value for minimum conductivity at V_{Dirac}, while, the dirty sample has lower mobility (lower slope), larger gate voltage offsets (far from $V_g = 0$), wider minimum conductivity plateau and there is electron and hole asymmetry can be explained by drift of charged impurities.

The carrier concentration becomes smaller than charged impurity density near the Dirac point, transport occurs either through the electron or hole channel because of breaking the system into puddles of holes and electrons cause a duality in tow dimensions which might describe the the asymmetry in $\sigma(V_g)$. For uncorrelated scatterers, the mobility depends inversely on the density of charged impurities, $1/\mu \propto n_{imp}$.

A density distribution induced by charged impurities in graphene, both negative and positive fluctuations are screened by graphene and the residual density n^* is responsible for minimum conductivity at Dirac point. Therefor, the value of minimum conductivity depends on impurity concentration on graphene surface, Martin an et. al. [50] showed that the electron and hole puddle form near the charge neutral point in graphene.

The gate-voltage-dependent conductivity $\sigma(V_g)$ was measured for the pristine device, and again after each current annealing interval. After several intervals, the device has experienced the highest current annealing in UHV that increased the graphene temperature up to $600°C$ to remove strongly adsorbed contaminants. figure 4.1 shows the conductivity versus gate voltage for the pristine graphene device before and after current annealing at room temperature in UHV.

After current annealing, (1) the mobility increases, (2) $\sigma(V_g)$ becomes less linear, (3) the mobility symmetry for holes versus electrons increases, (4) the gate voltage of minimum conductivity $V_{g,min}$ does not shift towards zero gate voltage, (5) the width of the minimum conductivity region in V_g narrows and (6) the minimum conductivity σ_{min} increases figure 4.1.

By considering the coupling constant α, defined as the ratio between the graphene coulomb potential and kinetic energy, which is the criterion of coupling between graphene and impurities,

$$\alpha = \frac{e^2}{\epsilon_0 \hbar \nu_F} \tag{4.4}$$

where e is the electric charge, ϵ_0 is the vacuum permittivity and $\hbar$ is Planck's constant. Graphene conductivity strongly depends on this coupling parameter α. For long rang impurities from Boltzmann transport theory [8]

$$\sigma_l = \frac{2e^2}{h} \frac{n}{F_l(\alpha) n_{imp}} \tag{4.5}$$

$$F_l(\alpha) = \pi \alpha^2 + 24\alpha^3(1 - \pi\alpha) + \frac{16\alpha^3(6\alpha^2 - 1)\arccos[1/2\alpha]}{\sqrt{4\alpha^2 - 1}} \tag{4.6}$$

The minimum conductivity σ_{min} can be estimated by considering the Boltzmann conductivity of residual density n^* (density of electron and hole puddles) induced by charge impurities,

$$\sigma_{min} = \frac{2e^2}{h} \frac{n^*(\alpha)}{F_l(\alpha) n_{imp}} \tag{4.7}$$

while $n^* = \langle V_D^2 \rangle / [\pi \hbar^2 \nu_f^2]$ and

$$\langle V_D^2 \rangle = n_{min} \hbar^2 \nu_f^2 \alpha^2 \int dq \left(\frac{e^{-qd}}{q\epsilon(q)} \right)^2 \tag{4.8}$$

where d is the impurity separation from graphne and $\epsilon(q)$ is the RPA dielectric function. Upon removing the ice layer, the mobility limited by long-range scattering (charged impurities) decreases because of increasing the coupling parameter α. The major effect on long-range scattering is, increasing the Coulomb interaction of electrons with charged impurities, increasing the scattering [51].

4.4 Short-range scattering in Graphene

Jang and et al [8] demonstrated that the dimensionless interaction strength α in graphene can be reduced by adding a water overlayer in graphene surface in ultrahigh vacuum, thereby increasing dielectric screening of impurity potential which limited the mobility by scattering the charge carriers. Owing to the background dielectric constant enhancement, the interaction between electrons and charged impurities is reduced and increased the mobility up to 30% and the carrier density decreased about 40%.

In graphene, electrons are confined to plane of atomic thickness with the electronic energy dispersion $E = \hbar\nu_F K$. Therefore, graphene properties can be tuned massively by its surrounding environment. The coupling constant α which is independent of carrier density, defines as the ratio between graphene coulomb potential and kinetic energy.

figure 4.2 shows the graphene sandwiched between tow dielectric with κ_1 and κ_2 dielectric constant [52],

$$\alpha = \frac{e^2}{(\kappa_1 + \kappa_2)\epsilon_0 \hbar \nu_F} \tag{4.9}$$

where $\nu_F = 10^6 m/s$ [17] is the Fermi velocity. Graphene is located on BN substrate with $\kappa_1 = 7.1$ [53] and water molecule $\kappa_2 = 3.2$ [54] on graphene, therefor $\alpha \approx 0.43$ and after current annealing by removing water molecules on graphene ($\kappa_2 = \kappa_{vac} = 1$) increasing α to 0.54 which increases the coupling between the graphene and impurities. The conductivity was measured using tow probe technique with an ac voltage of $50\mu V$ at $97.13Hz$ at a base pressure $\approx 10^{-10} torr$ at room temperature.

One such consequence is that graphene's properties may be tuned enormously by changing its surrounding environment. Jang and et al [8] showed that the removing the ice layers increases the α and conductivity limited by short range scatterers increases. By removing the ice layer, the atomic scale of short range potential does not modify by dielectric, but reduces the scattering resulting in conductivity.

$$\alpha = \frac{e^2}{\epsilon_0 \hbar \nu_F} \qquad\qquad \alpha = \frac{e^2}{(\kappa_1 + \kappa_2)\epsilon_0 \hbar \nu_F}$$
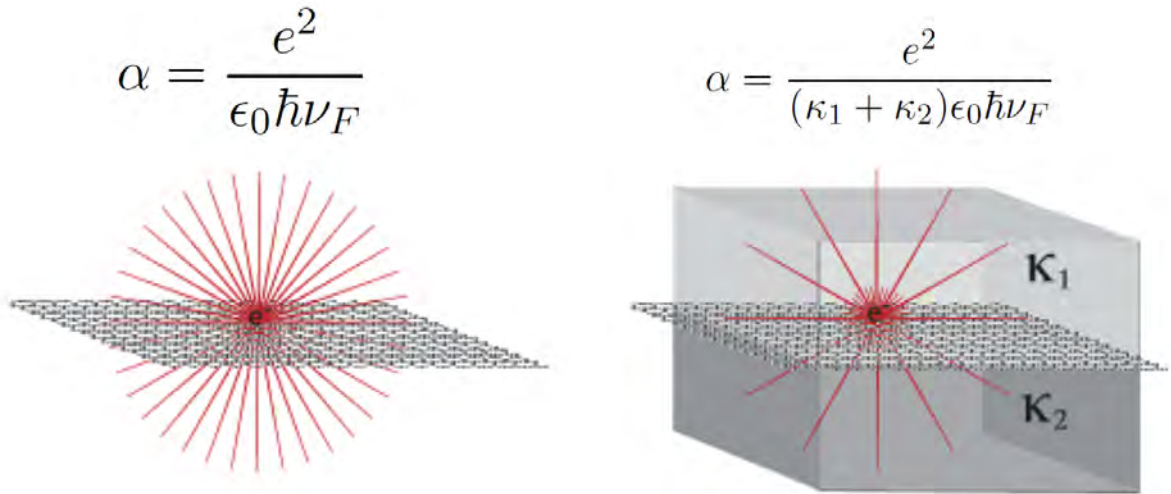
FIGURE 4.2: Dielectric environment on graphene which controls the interaction strength by the coupling constant α [8]

4.5 Results and Discussion

figure 4.1 shows the conductivity as a function of gate voltage before and after current annealing, we observed (1)the minimum conductivity dose not remain constant (2) the minimum V_g at minimum conductivity is changed (3)the maximum slope of $\sigma(V_g)$ is not steeper after current annealing. As the number of water molecules decreases, the mobility decreases.

There is an asymmetry between electrons and holes mobility that Novikov [45] suggested, repelling electrons by negative charge impurities results in slightly higher mobility for electrons since there are more negatively charge impurity centers [55].

Adsorbed contamination on graphene surface were removed by applying ultrahigh current density through a few microns wide graphene device. Annealing at several hundreds degree Celsius in Ar/H_2 environment removed the contamination, but, exposure the sample to air reintroduces contaminants and water. Applying a few volts across the sample (sample width $5\mu m$ and thickness of $0.35nm$) induce a hug current flow about $10mA$ which translates into large current density $\approx 5.7 \times 10^{12} A/m_2$. This hug current passing through the mesoscopic, conducting device figure 4.4 with the power of $\approx 40mW$ include electromigration and Joule heating increases the sample temperature. However, it is difficult to have a good estimation about the temperature on graphene surface, since most of the heat is evacuated by the gold electrodes.
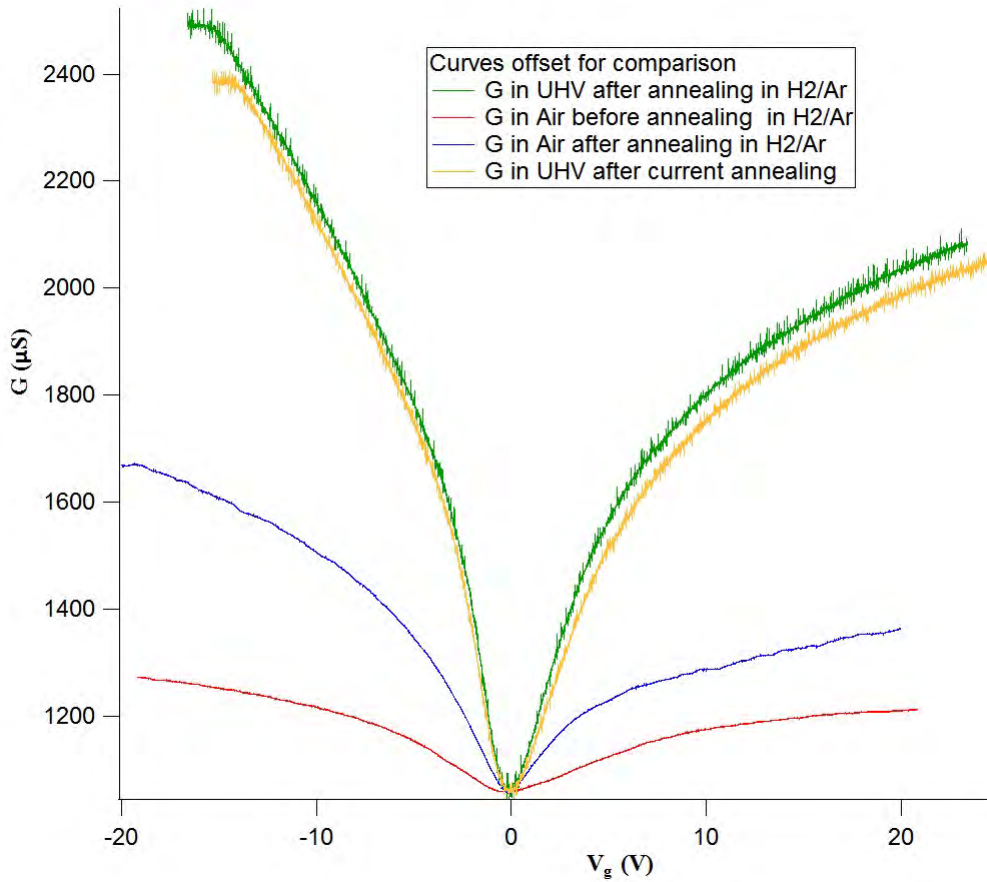
FIGURE 4.3: Conductance versus gate voltage, all the Dirac points moved to zero that make it possible to compare the mobility and conductance during the experiment

Current annealing remove the ice from the graphene surface and increases the coulomb interaction of electrons with charged impurities, increasing the scattering [51]. Competing between reduced mobility and increased carrier concentration in electron and hole puddles can keep the minimum conductivity unchanged but it does not happen in this case. In figure 4.3 all the Dirac points are moved to zero gate voltage to make it possible to compare the mobility and conductivity. After annealing the graphene in H_2/Ar mobility and conductivity were increased and we can see this increase after transferring the sample in UHV but there is a slight reduction after current annealing.

figure 4.5 shows the topographic STM scan of the sample before and after current annealing. The high temperature generated by the Joule heating, contamination might have melted and form a thin layer on the graphene, evaporated or sublimated. The temperature on graphene was estimated, that Mosre and et al [33, 56] used CdSe nanoparticles and considering the melting point of CdSe during the applying current, which should be more than $600°C$ in our sample at highest current. Moser and et al[33] showed that gold electrode act as heat sinks, owing to the remaining particles close to the electrodes.
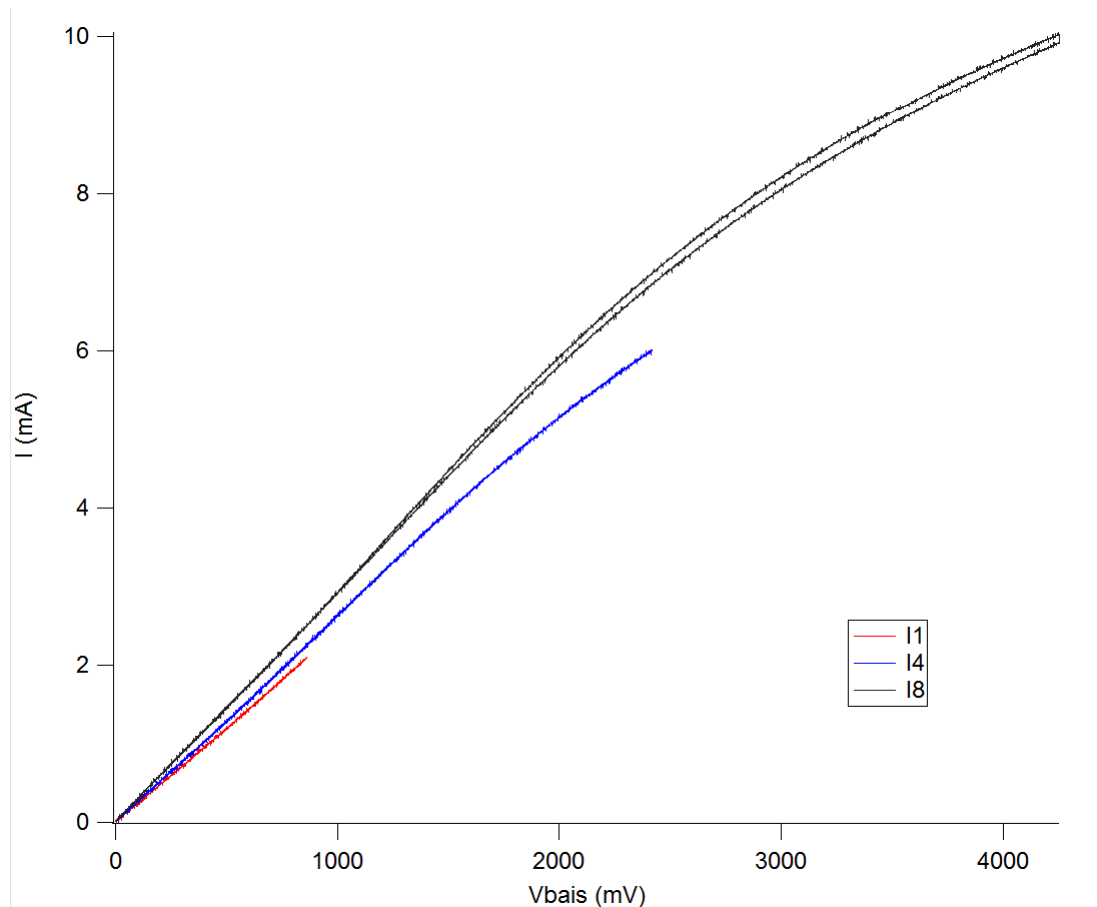
FIGURE 4.4: Voltage versus current applied trough the graphene flake, we increased the voltage until reach the given current and stayed at this voltage until the current drops in each current annealing interval

STM images figure 4.5 show the influence of electrical current on the morphology of graphene surface. Roughness has been measured at every points in the area $5\mu m \times 5\mu m$ figure 4.6 at the points vertical and horizontal lines cross each other, after every current annealing process. figure 4.5 shows the STM images from the middle point of this region. Typically, freshly graphene device transferred to the STM chamber an average roughness figure 4.5(a) $R_a = 8.5\mathring{A}$ is measured, suggesting the the presence of contamination on the graphene surface. Roughness was decreased by ramping up the voltage to 2V figure 4.4 in three steps figure 4.6(b) $R_b = 7\mathring{A}$. Roughness decreases as the voltage is further increased figure 4.5(c,d), $R_c = 4\mathring{A}$ and $R_d = 1\mathring{A}$ for $V_c = 3V$ and $V_d = 4V$. The average roughness did not change at the edges of scanning area $(5 \times 5\mu m)$which means closer to the gold electrodes is not getting hot and the gold electrodes play as heat sink for graphene flake.

The contaminants can dope the graphene and move the minimum conductivity far from the $V_b = 0$. These residues consist in part of non-dissolved PMMA and after cleaning in air, other adsorbents like oxygen molecules tend to counterbalance the surface charge.
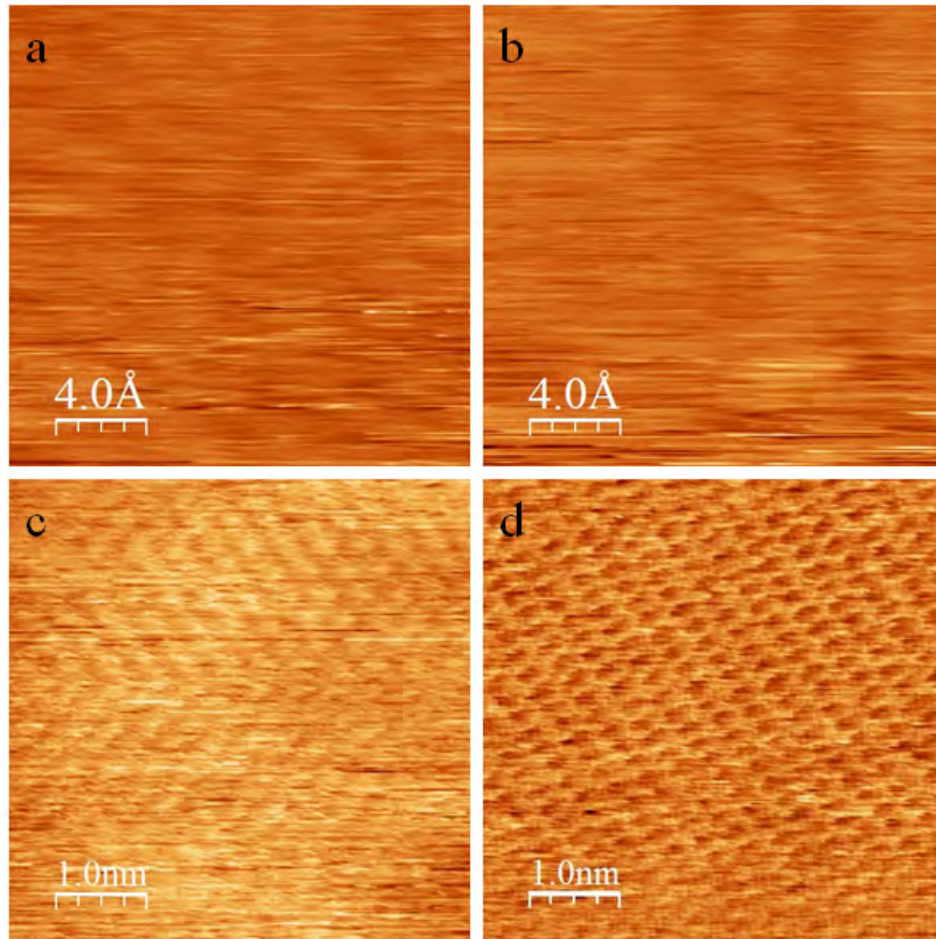
FIGURE 4.5: STM topography image (a) after transferring the graphene device in STM at $0.18nA$ and $-0.15V$ image size $2nm \times 2nm$ (b) after first current annealing $I1$ figure 4.4 at $0.15nA$ and $-0.15V$ image size $2nm \times 2nm$ (c) after fourth current annealing (d) after last current annealing $I8$ at $0.15nA$ and $-0.15V$ image size $5nm \times 5nm$

Charged impurity scattering and electron and hole puddles determine the minimum conductivity and long range scattering by charged impurities dominants at low carrier density [34, 42, 44, 55]. There is a competition between long-range scattering which is responsible for linear conductivity [38, 52] by changing the carrier density (constant mobility) and short-range scattering, giving a constant conductivity independent of carrier density. Also, the charged impurities were sublimated or evaporated during the current annealing.

Therefore, the dielectric environment and residual charged impurities can effect dramatically on transport on graphene. Conductivity on graphene depends on charged impurity (long-range scatterer) and ice layer (short-range scatterer). The minimum conductivity depends on charged impurity density, removing the long range scatterers, increasing the conductivity. Ice layers act as a short range scatterer and reduce the coupling between charged impurities and graphene in the other words, screen the strength of long range scatterers and increases the conductivity by this way, in contrast, more ice layers
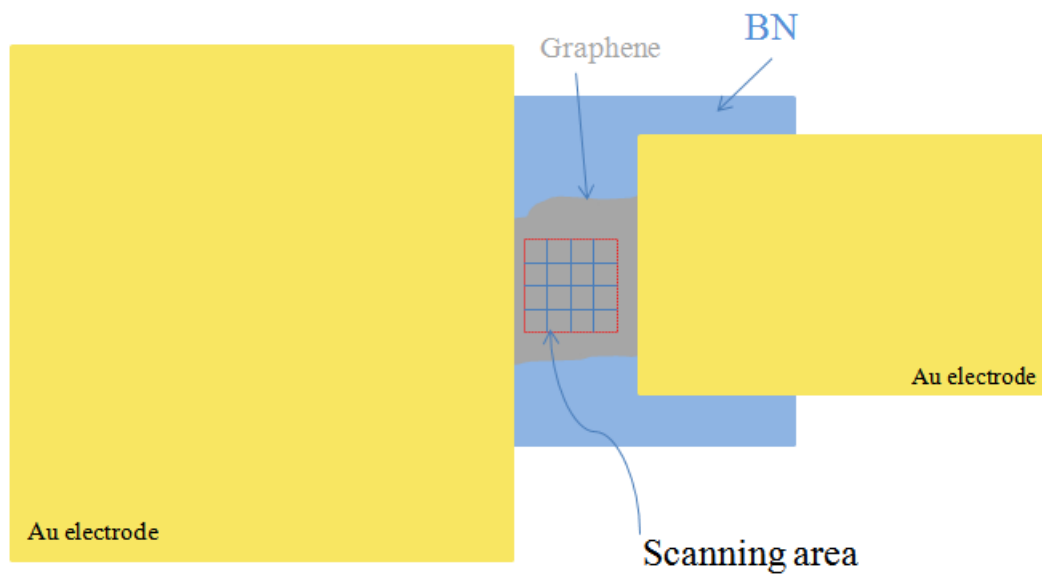
FIGURE 4.6: Scanning area on graphene, at each point that horizontal and vertical lines meet each other scanning has been done to have idea about the roughness in different regions and after current annealing

reduce the mobility in graphene. Therefor, removing ice layer and charged impurities simultaneously might change the conductivity dramatically.

Bibliography

[9] K S Novoselov, a K Geim, S V Morozov, D Jiang, Y Zhang, S V Dubonos, I V Grigorieva, and a a Firsov. Electric field effect in atomically thin carbon films. *Science (New York, N.Y.)*, 306(5696):666–9, October 2004. ISSN 1095-9203. doi: 10. 1126/science.1102896. URL http://www.ncbi.nlm.nih.gov/pubmed/15499015.

[10] D. S. L. Abergel, A. Russell, and Vladimir I. Fal'ko. Visibility of graphene flakes on a dielectric substrate. *Applied Physics Letters*, 91(6):063125, 2007. ISSN 00036951. doi: 10.1063/1.2768625. URL http://link.aip.org/link/APPLAB/v91/i6/p063125/s1&Agg=doi.

[11] P. Blake, E. W. Hill, a. H. Castro Neto, K. S. Novoselov, D. Jiang, R. Yang, T. J. Booth, and a. K. Geim. Making graphene visible. *Applied Physics Letters*, 91(6): 063124, 2007. ISSN 00036951. doi: 10.1063/1.2768624. URL http://link.aip.org/link/APPLAB/v91/i6/p063124/s1&Agg=doi.

[12] C Casiraghi, A Hartschuh, E Lidorikis, H Qian, H Harutyunyan, T Gokus, K S Novoselov, and a C Ferrari. Rayleigh imaging of graphene and graphene layers. *Nano letters*, 7(9):2711–7, September 2007. ISSN 1530-6984. doi: 10.1021/nl071168m. URL http://www.ncbi.nlm.nih.gov/pubmed/17713959.

[13] Xavier Blase Charlier, Jean-Christophe and Stephan Roche. Electronic and transport properties of nanotubes. *Reviews of Modern Physics*, 79(2):677–732, May 2007. ISSN 0034-6861. doi: 10.1103/RevModPhys.79.677. URL http://link.aps.org/doi/10.1103/RevModPhys.79.677.

[14] G. Dresselhaus Saito, R. and M. S. Dresselhaus. Physical properties of carbon nanotubes. *Imperial College Press, London*, 1(1):1, 1 1998. URL 1.

[15] W. Andreoni. The physics of fullerene-based and fullerene-related materials. *Springer, Berlin*, 1(1):1, 1 1. URL 1.

[16] P. R. Wallace. A simple extended-cavity diode laser. *Physical Review*, 69(0):622, 0 1998. URL http://link.aip.org/link/?RSI/69/1236/1.

[17] K S Novoselov, A K Geim, S V Morozov, D Jiang, M I Katsnelson, I V Grigorieva, S V Dubonos, and A A Firsov. Two-dimensional gas of massless Dirac fermions in graphene. *Nature*, 438(7065):197–200, November 2005. ISSN 1476-4687. doi: 10.1038/nature04233. URL http://www.ncbi.nlm.nih.gov/pubmed/16281030http://www.nature.com/nature/journal/v438/n7065/abs/nature04233.html.

[18] Yuanbo Zhang, Yan-wen Tan, Horst L Stormer, and Philip Kim. Experimental observation of the quantum Hall effect and Berry's phase in graphene. *Nature*, 438 (7065):201–4, November 2005. ISSN 1476-4687. doi: 10.1038/nature04235. URL http://www.ncbi.nlm.nih.gov/pubmed/16281031.

[19] K S Novoselov, Z Jiang, Y Zhang, S V Morozov, H L Stormer, U Zeitler, J C Maan, G S Boebinger, P Kim, and A K Geim. Room-temperature quantum Hall effect in graphene. *Science (New York, N.Y.)*, 315(5817):1379, March 2007. ISSN 1095-9203. doi: 10.1126/science.1137201. URL http://www.ncbi.nlm.nih.gov/pubmed/17303717.

[1] Nuno Miguel Peres Antonio Castro Neto, Francisco Guinea. Drawing conclusions from graphene, 2006. URL http://physicsworldarchive.iop.org/pdf?site=pwa&bkdir=19/11&pdf=phwv19i11a34&pdfhash=E77F683A60E2280744900CF39B91DB1F&doctime=Thu%2C14Nov201312%3A41%3A14GMT.

[2] Eva Y Andrei, Guohong Li, and Xu Du. Electronic properties of graphene: a perspective from scanning tunneling microscopy and magnetotransport. *Reports on progress in physics. Physical Society (Great Britain)*, 75(5):056501, May 2012. ISSN 1361-6633. doi: 10.1088/0034-4885/75/5/056501. URL http://www.ncbi.nlm.nih.gov/pubmed/22790587.

[3] M. Ali Omar. *Elementary solid state physics: principles and applications*.

[20] S. Reich, J. Maultzsch, C. Thomsen, and P. Ordejón. Tight-binding description of graphene. *Physical Review B*, 66(3):035412, July 2002. ISSN 0163-1829. doi: 10.1103/PhysRevB.66.035412. URL http://link.aps.org/doi/10.1103/PhysRevB.66.035412.

[21] R. Deacon, K.-C. Chuang, R. Nicholas, K. Novoselov, and A. Geim. Cyclotron resonance study of the electron and hole velocity in graphene monolayers. *Physical Review B*, 76(8):081406, August 2007. ISSN 1098-0121. doi: 10.1103/PhysRevB.76.081406. URL http://link.aps.org/doi/10.1103/PhysRevB.76.081406.

[4] a. H. Castro Neto, N. M. R. Peres, K. S. Novoselov, and a. K. Geim. The electronic properties of graphene. *Reviews of Modern Physics*, 81(1):109–162, January 2009.

ISSN 0034-6861. doi: 10.1103/RevModPhys.81.109. URL http://link.aps.org/doi/10.1103/RevModPhys.81.109.

[5] Edward Mccann. Electronic properties of monolayer and bilayer graphene. pages 1–40, 2012.

[22] Cristina Bena and Steven Kivelson. Quasiparticle scattering and local density of states in graphite. *Physical Review B*, 72(12):125432, September 2005. ISSN 1098-0121. doi: 10.1103/PhysRevB.72.125432. URL http://link.aps.org/doi/10.1103/PhysRevB.72.125432.

[23] J. P. Hobson and W. A. Nierenberg. The statistics of a two-dimensional, hexagonal net. *Phys. Rev.*, 89:662–662, Feb 1953. doi: 10.1103/PhysRev.89.662. URL http://link.aps.org/doi/10.1103/PhysRev.89.662.

[24] L. Landau. A simple extended-cavity diode laser. *Z. Phys*, 64(0):629, 0 1930. URL http://link.springer.com/article/10.1007/BF01397213.

[25] J. W. McClure. Diamagnetism of graphite. *Phys. Rev.*, 104:666–671, Nov 1956. doi: 10.1103/PhysRev.104.666. URL http://link.aps.org/doi/10.1103/PhysRev.104.666.

[26] Chun Hung Lui, Li Liu, Kin Fai Mak, George W Flynn, and Tony F Heinz. Ultraflat graphene. *Nature*, 462(7271):339–41, November 2009. ISSN 1476-4687. doi: 10.1038/nature08569. URL http://www.ncbi.nlm.nih.gov/pubmed/19924211.

[27] Masa Ishigami, J H Chen, W G Cullen, M S Fuhrer, and E D Williams. Atomic structure of graphene on SiO2. *Nano letters*, 7(6):1643–8, June 2007. ISSN 1530-6984. doi: 10.1021/nl070613a. URL http://www.ncbi.nlm.nih.gov/pubmed/17497819.

[28] C R Dean, a F Young, I Meric, C Lee, L Wang, S Sorgenfrei, K Watanabe, T Taniguchi, P Kim, K L Shepard, and J Hone. Boron nitride substrates for high-quality graphene electronics. *Nature nanotechnology*, 5(10):722–6, October 2010. ISSN 1748-3395. doi: 10.1038/nnano.2010.172. URL http://www.ncbi.nlm.nih.gov/pubmed/20729834.

[6] Régis Decker, Yang Wang, Victor W Brar, William Regan, Hsin-zon Tsai, Qiong Wu, William Gannett, Alex Zettl, and Michael F Crommie. Local electronic properties of graphene on a BN substrate via scanning tunneling microscopy. *Nano letters*, 11(6):2291–5, June 2011. ISSN 1530-6992. doi: 10.1021/nl2005115. URL http://www.ncbi.nlm.nih.gov/pubmed/21553853.

[29] Jairo Velasco. *Investigation of Single Particle and Many Body Physics in Dual-Gated 1,2,3 Layers of Graphene A*. PhD thesis, UC Riverside, 2012. URL http://escholarship.org/uc/item/8z2321gj.

[30] G. Binning, H. Rohrer, Ch. Gerber, and E. Weibel. Surface studies by scanning tunneling microscopy. *Phys. Rev. Lett.*, 49:57–61, Jul 1982. doi: 10.1103/PhysRevLett. 49.57. URL http://link.aps.org/doi/10.1103/PhysRevLett.49.57.

[7] Guohong Li, Adina Luican, and Eva Y Andrei. Self-navigation of a scanning tunneling microscope tip toward a micron-sized graphene sample. *The Review of scientific instruments*, 82(7):073701, July 2011. ISSN 1089-7623. doi: 10.1063/1.3605664. URL http://www.ncbi.nlm.nih.gov/pubmed/21806183.

[31] Elena Stolyarova, Kwang Taeg Rim, Sunmin Ryu, Janina Maultzsch, Philip Kim, Louis E Brus, Tony F Heinz, Mark S Hybertsen, and George W Flynn. High-resolution scanning tunneling microscopy imaging of mesoscopic graphene sheets on an insulating surface. *Proceedings of the National Academy of Sciences of the United States of America*, 104(22):9209–12, May 2007. ISSN 0027-8424. doi: 10.1073/pnas. 0703337104. URL http://www.pubmedcentral.nih.gov/articlerender.fcgi?artid=1874226&tool=pmcentrez&rendertype=abstract.

[32] Masa Ishigami, J H Chen, W G Cullen, M S Fuhrer, and E D Williams. Atomic structure of graphene on SiO2. *Nano letters*, 7(6):1643–8, June 2007. ISSN 1530-6984. doi: 10.1021/nl070613a. URL http://www.ncbi.nlm.nih.gov/pubmed/17497819.

[33] J. Moser, A. Barreiro, and A. Bachtold. Current-induced cleaning of graphene. *Applied Physics Letters*, 91(16):163513, 2007. ISSN 00036951. doi: 10.1063/1. 2789673. URL http://link.aip.org/link/APPLAB/v91/i16/p163513/s1&Agg=doi.

[34] Y.-W. Tan, Y. Zhang, K. Bolotin, Y. Zhao, S. Adam, E. H. Hwang, S. Das Sarma, H. L. Stormer, and P. Kim. Measurement of Scattering Rate and Minimum Conductivity in Graphene. *Physical Review Letters*, 99(24):246803, December 2007. ISSN 0031-9007. doi: 10.1103/PhysRevLett.99.246803. URL http://link.aps.org/doi/10.1103/PhysRevLett.99.246803.

[35] J.-H. Chen, M. Ishigami, C. F, D.R. Hines, M.S. Fuhrer, and E.D. Williams. Printed Graphene Circuits. *Advanced Materials*, 19(21):3623–3627, November 2007. ISSN 09359648. doi: 10.1002/adma.200701059. URL http://doi.wiley.com/10.1002/adma.200701059.

[36] Sungjae Cho and Michael Fuhrer. Charge transport and inhomogeneity near the minimum conductivity point in graphene. *Physical Review B*, 77(8):081402, February 2008. ISSN 1098-0121. doi: 10.1103/PhysRevB.77.081402. URL http://link.aps.org/doi/10.1103/PhysRevB.77.081402.

[37] Eun-Ah Kim and a. H. Castro Neto. Graphene as an electronic membrane. *EPL (Europhysics Letters)*, 84(5):57007, December 2008. ISSN 0295-5075. doi: 10.1209/0295-5075/84/57007. URL http://stacks.iop.org/0295-5075/84/i=5/a=57007?key=crossref.b3267b2c635dc20c28d136943d428c1a.

[38] Tsuneya Ando. Screening Effect and Impurity Scattering in Monolayer Graphene. *Journal of the Physics Society Japan*, 75(7):074716, July 2006. ISSN 0031-9015. doi: 10.1143/JPSJ.75.074716. URL http://jpsj.ipap.jp/link?JPSJ/75/074716/.

[39] Kentaro Nomura and a. H. MacDonald. Quantum Transport of Massless Dirac Fermions. *Physical Review Letters*, 98(7):076602, February 2007. ISSN 0031-9007. doi: 10.1103/PhysRevLett.98.076602. URL http://link.aps.org/doi/10.1103/PhysRevLett.98.076602.

[40] K. Ziegler. Robust Transport Properties in Graphene. *Physical Review Letters*, 97(26):266802, December 2006. ISSN 0031-9007. doi: 10.1103/PhysRevLett.97.266802. URL http://link.aps.org/doi/10.1103/PhysRevLett.97.266802.

[41] N. Peres, F. Guinea, and A. Castro Neto. Electronic properties of disordered two-dimensional carbon. *Physical Review B*, 73(12):125411, March 2006. ISSN 1098-0121. doi: 10.1103/PhysRevB.73.125411. URL http://link.aps.org/doi/10.1103/PhysRevB.73.125411.

[42] Shaffique Adam, E H Hwang, V M Galitski, and S Das Sarma. A self-consistent theory for graphene transport. *Proceedings of the National Academy of Sciences of the United States of America*, 104(47):18392–7, November 2007. ISSN 1091-6490. doi: 10.1073/pnas.0704772104. URL http://www.pubmedcentral.nih.gov/articlerender.fcgi?artid=2141788&tool=pmcentrez&rendertype=abstract.

[43] Vadim Cheianov and Vladimir Fal'ko. Friedel Oscillations, Impurity Scattering, and Temperature Dependence of Resistivity in Graphene. *Physical Review Letters*, 97(22):226801, November 2006. ISSN 0031-9007. doi: 10.1103/PhysRevLett.97.226801. URL http://link.aps.org/doi/10.1103/PhysRevLett.97.226801.

[44] E. Hwang, S. Adam, and S. Sarma. Carrier Transport in Two-Dimensional Graphene Layers. *Physical Review Letters*, 98(18):186806, May 2007. ISSN 0031-9007. doi: 10.1103/PhysRevLett.98.186806. URL http://link.aps.org/doi/10.1103/PhysRevLett.98.186806.

[45] D. S. Novikov. Numbers of donors and acceptors from transport measurements in graphene. *Applied Physics Letters*, 91(10):102102, 2007. ISSN 00036951. doi: 10.1063/1.2779107. URL http://link.aip.org/link/APPLAB/v91/i10/p102102/s1&Agg=doi.

[46] Maxim Trushin and John Schliemann. Minimum Electrical and Thermal Conductivity of Graphene: A Quasiclassical Approach. *Physical Review Letters*, 99(21): 216602, November 2007. ISSN 0031-9007. doi: 10.1103/PhysRevLett.99.216602. URL http://link.aps.org/doi/10.1103/PhysRevLett.99.216602.

[47] Jun Yan, Yuanbo Zhang, Philip Kim, and Aron Pinczuk. Electric Field Effect Tuning of Electron-Phonon Coupling in Graphene. *Physical Review Letters*, 98 (16):166802, April 2007. ISSN 0031-9007. doi: 10.1103/PhysRevLett.98.166802. URL http://link.aps.org/doi/10.1103/PhysRevLett.98.166802.

[48] a K Geim and K S Novoselov. The rise of graphene. *Nature materials*, 6(3):183–91, March 2007. ISSN 1476-1122. doi: 10.1038/nmat1849. URL http://www.ncbi.nlm.nih.gov/pubmed/17330084.

[49] Xin-Zhong Yan, Yousef Romiah, and C. S. Ting. Electric transport theory of dirac fermions in graphene. *Phys. Rev. B*, 77:125409, Mar 2008. doi: 10.1103/PhysRevB.77.125409. URL http://link.aps.org/doi/10.1103/PhysRevB.77.125409.

[50] J Martin, N Akerman, G Ulbricht, T Lohmann, J. H. Smet, K. von Klitzing, and A. Yacoby. Observation of electron–hole puddles in graphene using a scanning single-electron transistor. *Nature Physics*, 4(2):144–148, November 2007. ISSN 1745-2473. doi: 10.1038/nphys781. URL http://www.nature.com/nphys/journal/v4/n2/abs/nphys781.htmlhttp://www.nature.com/doifinder/10.1038/nphys781.

[8] C. Jang, S. Adam, J.-H. Chen, E. D. Williams, S. Das Sarma, and M. S. Fuhrer. Tuning the Effective Fine Structure Constant in Graphene: Opposing Effects of Dielectric Screening on Short- and Long-Range Potential Scattering. *Physical Review Letters*, 101(14):146805, October 2008. ISSN 0031-9007. doi: 10.1103/PhysRevLett.101.146805. URL http://link.aps.org/doi/10.1103/PhysRevLett.101.146805.

[51] Debdeep Jena and Aniruddha Konar. Enhancement of carrier mobility in semiconductor nanostructures by dielectric engineering. *Phys. Rev. Lett.*, 98:136805, Mar 2007. doi: 10.1103/PhysRevLett.98.136805. URL http://link.aps.org/doi/10.1103/PhysRevLett.98.136805.

[52] N. Peres, F. Guinea, and A. Castro Neto. Coulomb interactions and ferromagnetism in pure and doped graphene. *Physical Review B*, 72(17):174406, November 2005. ISSN 1098-0121. doi: 10.1103/PhysRevB.72.174406. URL http://link.aps.org/doi/10.1103/PhysRevB.72.174406.

[53] P. J. Gielisse, S. S. Mitra, J. N. Plendl, R. D. Griffis, L. C. Mansur, R. Marshall, and E. A. Pascoe. Lattice infrared spectra of boron nitride and boron monophosphide. *Phys. Rev.*, 155:1039–1046, Mar 1967. doi: 10.1103/PhysRev.155.1039. URL http://link.aps.org/doi/10.1103/PhysRev.155.1039.

[54] V. F. Petrenko and R.W. Whitworth. The physics of ice. *Oxford University, Oxford, England,*, page 1.

[55] J.-H. Chen, C. Jang, S. Adam, M. S. Fuhrer, E. D. Williams, and M. Ishigami. Charged-impurity scattering in graphene. *Nature Physics*, 4(5):377–381, April 2008. ISSN 1745-2473. doi: 10.1038/nphys935. URL http://www.nature.com/doifinder/10.1038/nphys935.

[56] a N Goldstein, C M Echer, and a P Alivisatos. Melting in semiconductor nanocrystals. *Science (New York, N.Y.)*, 256(5062):1425–7, June 1992. ISSN 0036-8075. doi: 10.1126/science.256.5062.1425. URL http://www.ncbi.nlm.nih.gov/pubmed/17791609.